Doctoral Dissertation
博士論文

Regulation of meiotic recombination initiation by a conserved HORMAD protein Hop1.

(保存された HORMAD 型染色体因子 Hop1 による組換え開始制御機構)

A Dissertation Submitted for Degree of Doctor of Philosophy
December 2018

平成３０年１２月博士(理学)申請

Department of Biological Sciences, Graduate School of Science,
The University of Tokyo

東京大学大学院理学系研究科生物科学専攻

Ryo Kariyazono
仮屋園　遼

Table of contents

Abstract

Meiotic recombination is essential for the diversification of genetic information and the precise chromosome segregation during meiosis. Meiotic recombination is initiated by the programmed formation of DNA double strand breaks (DSBs), which are repaired by homologous recombination between homologous chromosomes (homologues). DSBs are introduced by an evolutionally-conserved meiosis-specific topoisomerase-like Spo11 protein, under the regulation by multi-layered mechanisms.

The meiotic chromosome comprises higher order structures called “axis” and “loop”. Activities of Spo11 complex are controlled by axis, and Spo11 complex introduce DSB on the loop region. However, the mechanisms underlying interaction of Spo11 complex to the axis and loops still remain elusive.

In this study, I demonstrate that *Schizosaccharomyces pombe* axis protein Hop1 can interact with both Spo11 component protein Rec15/Mer2/IHO1 and an axis protein Rec10/Red1/SYCP2, thereby facilitating robust axial localization of Spo11 complex and DSB formation. Genetic studies using separation-of-function mutations, yeast two/three hybrid experiments, and immunoprecipitation assays supported the notion that Rec10, Hop1, and Rec15 mutually interact with each other. Taken together, I propose that Hop1 serves as a molecular matchmaker for interaction between Rec15 and Rec10 to enhance interaction between Spo11 complex and axial proteins thereby promoting DSB formation.

Abbreviations

AE	axial element
BSA	bovine serum albumin
CDK	cyclin dependent kinase
ChIP	chromatin immunoprecipitation
ChIP-chip	chromatin immunoprecipitation on microarrays
ChIP-seq	chromatin immunoprecipitation sequencing
CO	crossover
DDK	Dbf4 dependent kinase
DSB	double strand break
EDTA	ethylene diamine tetraacetic acid
EGTA	ethylene glycol tetraacetic acid
EMM	Edinburgh minimal medium
HEPES	4-(2-hydroxyethyl)-1-piperazineethanesulfonic acid
MNase	Micrococcal nuclease
MOPS	3-(N-morpholino)propanesulfonic acid
NCO	non crossover
PBS	phosphate buffered saline
PIPES	iperazine-1,4-bis(2-ethanesulfonic acid)
PMSF	phenylmethylsulfonyl fluoride
SD	synthetic defined medium
SC	synaptonemal complex
Tris	tris-hydroxymethyl-aminomethane
Y2H	yeast 2 hybrid assay
Y3H	yeast 3 hybrid assay

1. Introduction

1.1 Meiotic recombination and double strand breaks (DSBs)

Meiosis is a crucial step for the reproduction of eukaryotes. During meiosis, diploid cells reduce their genome set by half to produce haploid gametes, by performing one round of DNA replication followed by two sequential rounds of nuclear divisions (Figure 1A).

One of the most crucial steps in meiosis is the meiotic recombination, which is essential for diversifying genomes and precise chromosome segregation. Meiotic recombination is initiated by the fromation of double strand breaks (DSBs) on DNA. In meiotic recombination, some of introduced DSBs are repaired via homologous DNA sequences in the sister chromatid (intersister recombination), but the majority of DSBs is repaired by using homologous DNA sequences in homologues (interhomolog recombination).

Meiotic homologous recombination is categorized into two types: the reciprocal exchange of DNA strands around DSB site (crossovers, CO) or non-reciprocal exchange (Non-crossovers, NCO), depending on the states of recombination intermediates (Figure 1B). COs between homologous chromosomes provide physical linkages between homologs in addition to sister chromatid cohesion. Such physical connections between homologues plays critical roles in proper segregation of meiotic chromosomes into gamates.

1.2 Meiotic chromosome structure and recombination

DSB formation and recombination are governed by meiosis specific chromosome structure. Microscopic observations and Hi-C (high-dimensional chromosome conformation capture combined with high-throughput DNA sequencing) data have revealed that the meiotic chromosome is organized into the linear arrays of chromatin loops anchored to the axis (Blat et al., 2002; Muller et al., 2018; Sym et al., 1993) (Figure 2A).

In the axes, proteinaceous structures called axial elements (AEs) are formed. AEs are further assembled into synaptonemal complexes (SCs), which are formed between paired homologs during meiosis. The formation of AEs require Rec8, a kleisin-subunit of meiotic cohesin, which is loaded on the chromatin during DNA replication. (Kitajima et al., 2003; Lin et al., 1992; Molnar et al., 1995; Watanabe and Nurse 1999). Genome-wide distribution analysis using chromatin immunoprecipitation (ChIP) and ChIP-DNA chip (ChIP-chip)/ChIP-sequencing (ChIP-seq) revealed that Rec8 is localized at discrete positions along meiotic chromosome arms as well as pericentromeric regions (Ding et al., 2006; Ito et al., 2014; Klein et al. 1999; Kugou et al., 2009; Ludin et al., 2008; Molnar 2003; Xu et al., 2005). These Rec8 binding sites on chromosome arms are assumed to be overlapping with potential chromosomal axis sites.

AEs are also enriched with several other protein components, such as Red1 and Hop1 in budding yeast. Axis proteins have multiple integrated roles in the regulation of meiotic recombination, such as enhancing DSB formation (Hollingsworth and Byers 1989; Rockmill and Roeder 1988, 1991), bias for inter-homologous recombination rather than inter-sister

recombination (Kim et al., 2010; Niu et al., 2005), and promoting COs rather than NCOs (Brown et al., 2018; Medhi et al., 2016), meiotic recombination checkpoint. (Carballo et al., 2008; Xu, Weiner, and Kleckner 1997). However, the precise molecular mechanisms of the regulation by those axial proteins have not yet been fully elucidated.

1.3 Spo11 complex: the conserved DSB processing machinery

DSBs are catalyzed by a conserved meiosis-specific type II topoisomerase-like protein Spo11 (Bergerat et al., 1997; Keeney et al., 1997). Spo11 functions as a complex, which consists of several conserved partner proteins. Series of studies revealed that the complex can be categorized into at least three distinct subgroups: 1) Topoisomerase VIB-like (Spo11-TOPVIBL) subunit; 2) DSB regulatory complex; 3) DSB formation/processing complex. In budding yeast *Saccharomyces cerevisiae*, the first group consists of Spo11, Ski8, Rec102 and Rec104, the DSB regulatory complex is composed of Rec114-Mei4-Mer2 (RMM) proteins, and the DSB formation/processing complex consists of Mre11-Rad50-Xrs2 (MRX) proteins (Lam and Keeney, 2015). Those DSB-related proteins are conserved among eukaryotic species, although their primary sequences and the necessity for DSB formation are variable (see Table 1).

1.4 Regulation of DSBs

DSB formation is strictly controlled at temporal, quantitative and spatially by multi-layered mechanisms such as timing control in coupled with DNA replication, assembly of protein complexes, local chromatin structures, and high-order architecture of meiotic chromosomes.

1.4.1 Temporal regulation of DSBs

First, the timing of DSB introduction is strictly controlled in a cell cycle-dependent manner. DSB introduction and chiasma formation take place strictly after DNA replication. The molecular mechanisms of this regulation have been well studied in *S. cerevisiae* and *Schizosaccharomyces pombe*. In *S. cerevisiae,* during DNA replication, cyclin dependent kinase (CDK) and Dbf1 dependent kinase (DDK), the activator of replication complex, phosphorylates Mer2 in RMM complex (see chapter 1.2 and table 1). The phosphorylation enables Mer2 to interact with other DSB factors and thereby facilitating formation of the Spo11 complex. Such mechanisms ensure the occurrence of DSB formation after DNA replication. (Henderson et al., 2006; Murakami and Keeney, 2014; Sasanuma et al., 2008). In *S. pombe*, a meiosis-specific protein Mde2 is expressed after the completion of DNA replication. Mde2 stabilizes SFT complex (counterpart of RMM complex in *S. cerevisiae*) and bridges SFT with Rec6-Rec12-Rec14 DSB catalytic core sub-complex, leading to the stable formation of Spo11 complex and DSB formation (Miyoshi et al., 2012).

Another important factor of DSB regulation is higher-order chromosome architecture such as

axis and loop structures. The chromosome axis serves as the scaffold for the recombination machinery including Spo11 complex (Panizza et al., 2011). Since the axis formation requires DNA replication, Spo11 complex is not efficiently recruited to chromosome axis prior to DNA replication. This was demonstrated by ChIP experiments showing that Spo11 is initially recruited around the pericentromeric and Rec8 binding sites (Kugou et al., 2009; Ludin et al., 2008).

1.4.2 Quantitative regulation of DSBs

DSB formation is also quantitatively regulated by DNA damage checkpoint pathways. Upon DSB formation, ATM and ATR kinase are activated. In *S. cerevisiae*, ATM and ATR phosphorylate Rec114 in RMM complex, which results in repression of DSB catalytic activity (Carballo et al., 2013). ATM is also involved in “DSB homeostasis”, in which occurrence of a DSB suppress DSB formation at the adjacent recombination hotspots. ATM mediated local DSB interference exerts within a chromatin loop domain, suggesting axis-loop structure involves in the quantitative regulation of DSB by higher-order chromosome structures (Garcia et al., 2015).

1.4.3 Spatial regulation of DSBs

DSBs are preferentially introduced at discrete sites called DSB hotspots. Distribution of DSB hotspots has been studied in various taxa. Intensive studies in budding yeast revealed that DSB

hotspots are often found in gene promoters, especially region exhibiting constitutively open chromatin configuration (Wu and Lichten, 1994; Ohta et al., 1994). However, the accessibility is not sufficient for determining DSB hotspot, but Histone H3K4 tri-methyl modification also serves as the signature of DSB hotspot and the disruption of this modification results in a significant decrease in the DSB number (Borde et al., 2009).

In *S. pombe*, H3K9 acetylation is the primary epigenetic mark for DSB formation (Yamada et al., 2004; Yamada, Ohta, and Yamada, 2013). In both species, most DSB hotspots are observed in open chromatin regions. In mouse and human, hotspots are determined by sequence-specific DNA-binding PRDM9 protein, which has the Zinc-finger domains and the histone lysine-methyltransferase domain (Baudat et al., 2010).

Furthermore, the distribution of DSB hotspot is influenced by the positioning of the axis. High-throughput sequencing of Spo11-oligo DNA (a DSB repair intermediates consisting of covalently-linked Spo11-DSB complex) revealed that DSB formation occurs predominantly in loop regions (Neale et al., 2005; Pan et al., 2011). Therefore, distributions of DSB hotspots in loops and the axis-bound Rec8 sites show clear anti-correlation in budding and fission yeasts (Ludin et al., 2008; Ito et al., 2014). Consistently, Spo11 is detected in chromosomal loop regions, although it is initially recruited around pericentromeric and Rec8 binding sites (Kugou et al., 2009).

1.5 The interaction of chromosome axis and DSB mercenary

As already mentioned, Spo11 complex is initially recruited to the axis, while DSB hotspots are located in regions distant from the axis sites. Correspondingly, Spo11 and its partner proteins are transiently colocalized at both axis sites and DSB hotspots in loops in budding and fission yeasts (Grey et al., 2018; Miyoshi et al., 2012; Panizza et al., 2011).

Such localization pattern of Spo11 complex can be explained by the "tethered loop/axis complex (TLAC) model" (Blat et al., 2002; Kleckner, 2006; Zickler and Kleckner, 2015). In this model, DSB hotspots in loops can transiently interact with the chromosome axis to activate protein complexes for DSB formation (Figure 2A), though it is difficult to observe the direct interaction between the axis and loops.

Series of works in various taxa revealed a conserved feature of the molecular interaction, which helps Spo11 to localize in both the axis and DSB hotspots (Figure 2B). In budding yeast, localization of Spo11 in the axis and DSB hotspots depends on RMM complex. AE components Red1 and Hop1 are essential for the recruitment of Mer2 (a RMM complex component) to the axis, though interaction between Mer2 and Red1 or Hop1 has not been fully elucidated. Spo11 binds to DSB hotspot regions after the recruitment of RMM proteins to the axis, via interactions between Mer2 and Spp1, a component of the COMPASS histone H3K4 methyltransferase complex (Acquaviva et al., 2013).

In fission yeast, Spo11 orthologue Rec12 is localized to the axis and hotspot sites, with the help of SFT complex (counterpart of RMM complex in budding yeast). Rec15 in SFT complex is the counterpart of Mer2 in budding yeast and responsible for the axial localization of Rec12 complex via interaction with the axial protein Rec10 (fission yeast Red1 orthologue) (Miyoshi et al., 2012). The molecular interaction underlying interaction between Rec12 complex and DSB hotspot site is still elusive.

In *Mus musculus*, Mer2/Rec15 homolog IHO1 interacts with AE component HORMAD1 (yeast hop1 homolog). Deficiency in HORMAD1 partially affects localization pattern of IHO1 and other

proteins in spo11 complex (Stanzione et al., 2016). It should be noted that putative Red1/Rec10 homolog is axial element protein SYCP2, but its roles in localization of Spo11 complex is not uncovered.

1.6 Overview of this study

Subunits of Spo11 complex and several AE components are conserved among spices. Then the question arises whether the mechanisms of Spo11 complex to localize chromosome axis are conserved. To answer this question, I focused on axis-bound Hop1/HORMAD1 proteins. Hop1 proteins in many organisms share a highly conserved HORMA domain (Kim et al., 2014; Rosenberg and Corbett, 2015), which was also found in other important chromosomal proteins, such as Rev7 (an accessory subunit of DNA polymerase zeta) and Mad2 (an essential spindle checkpoint protein). Mad2 and Rev7 are reported to function as regulators with conformational switches for various chromosomal functions (Rosenberg and Corbett, 2015).

Hop1 is involved in various steps in meiosis in wide range of species. Deletion mutants of Hop1 orthologous in various organisms including budding yeast, fission yeast, nematode, and mammals, commonly lead to deficiency in DSB formation, despite the difference in the levels of deficiency. Hop1 is thus thought to be important for meiotic DSB formation (Couteau and Zetka, 2005; Daniel et al., 2011; Latypov et al., 2010; Mao-Draayer et al., 1996). Hop1 is also essential for SC formation in budding yeast, nematode, and mammals (Couteau et al., 2004; Daniel et al., 2011; Hollingsworth, Goetsch, and Byers, 1990). Budding yeast and mammalian

Hop1/HORMAD1 is dissociated from chromosomal regions where synapsis are completed (Borner et al., 2008; Fukuda et al., 2010; Joshi et al., 2009; Wojtasz et al., 2009). In addition, budding yeast Hop1 is involved in the recombination checkpoint and the recombination bias towards inter-homolog (Kim et al., 2010; Niu et al., 2005) as well as the CO/NCO pathway choice (Brown et al., 2018; Medhi et al., 2016).

In order to reveal the mechanisms of DSB formation governed by Hop1, I analysed Hop1 in fission yeast *S. pombe*. In *S. pombe*, Hop1 is involved in DSB formation as in other organisms, but most of other Hop1 functions are missing, because the developed SC structure is absent, and its regulatory function is also lacking. Nonetheless, Hop1 is important for DSB formation in *S. pombe* (Latypov et al., 2010; Rothenberg et al., 2009). The simplified function of *S. pombe* Hop1 enables us to focus on its roles in meiotic DSB formation.

In this study, I conducted ChIP and ChIP-seq analyses, protein interaction assays, and point-mutant studies to demonstrate that fission yeast Hop1 binds to Rec15 and Rec10, which promotes interaction between Spo11 complex and axis component, elucidating the conserved HORMA domain-containing protein-dependent mechanisms for axial localization of Spo11 complex and DSB formation.

1.7 Figures and tables of introduction

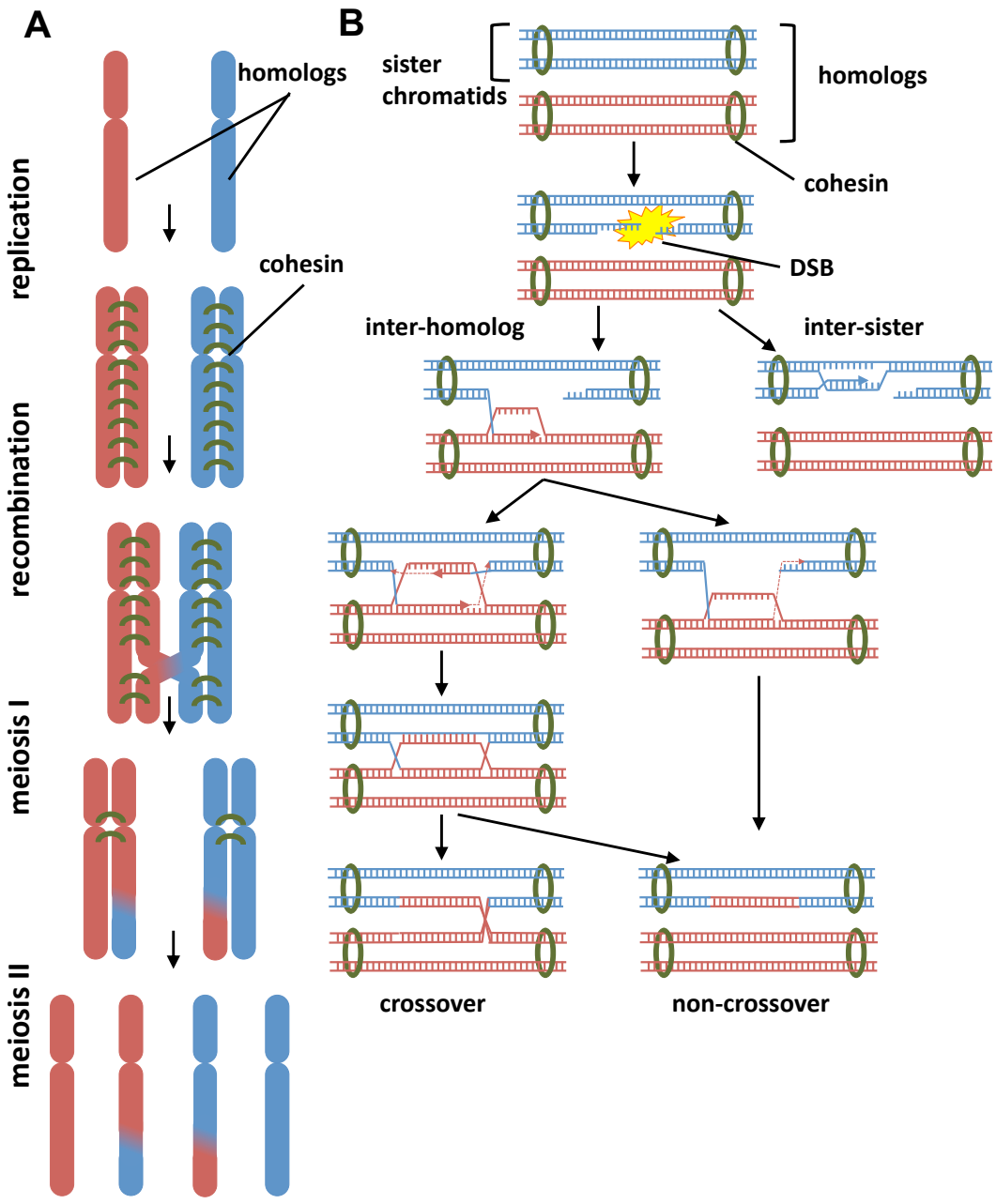

Figure 1

(A) Schematic diagram of the dynamics chromosomes during meiosis. (B) Schematic diagram of recombination between homologous or sister chromatids.

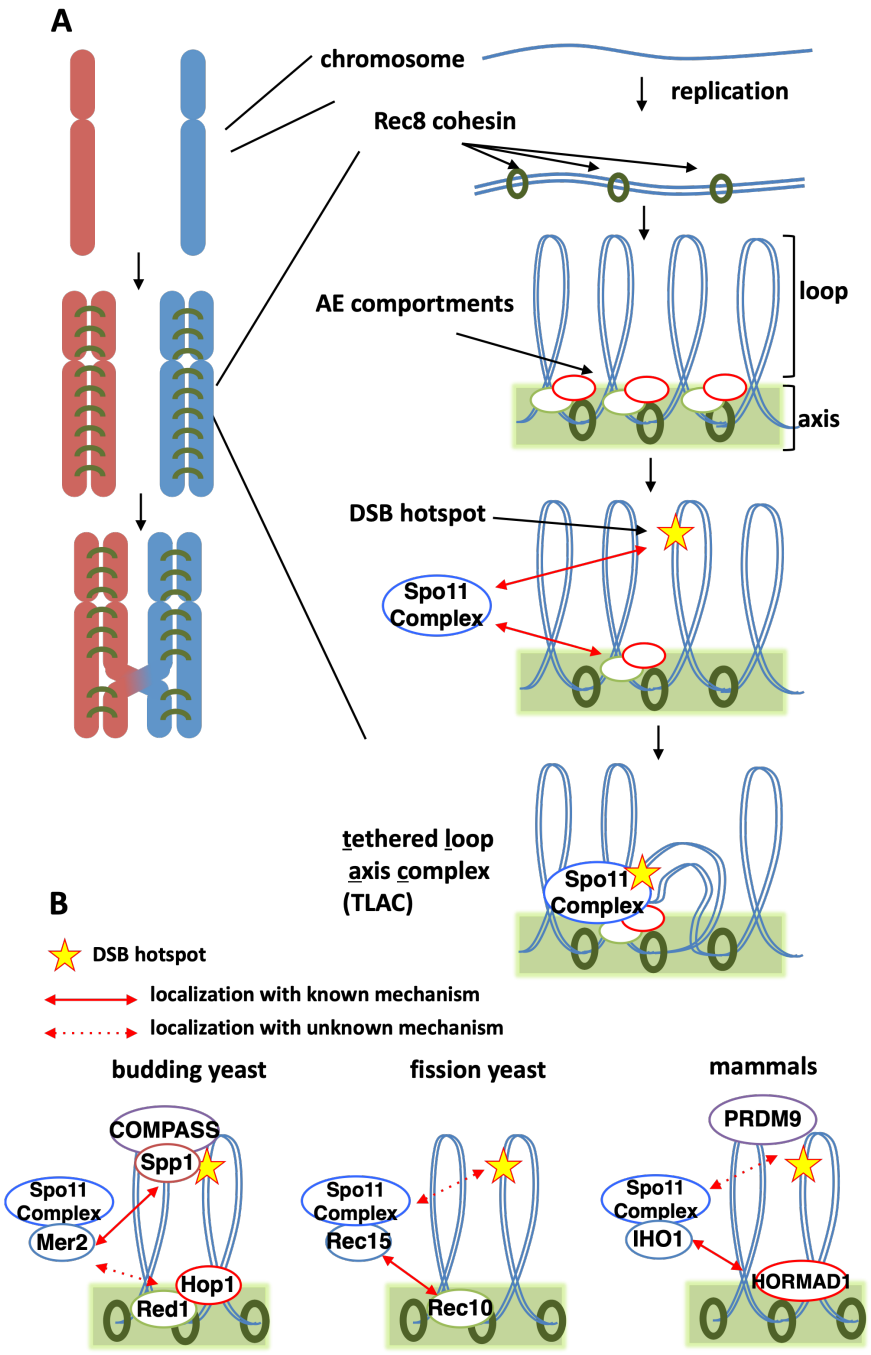

Figure 2

(A) The schematic drawing of meiotic chromosome structures established after replication. Note that Spo11 complex becomes activated after the formation of tethered loop axis complex (TLAC). (B) Molecular mechanism of TLAC model form previous studies in fission yeast, budding yeast and mammals. Solid red arrow indicates reported molecular interactions and dotty red arrow indicates interaction with unknown molecular interaction.

Table 1 Conservation of subunits in Spo11 complex

S. cerevisiae	*S. pombe*	*M. musculus*	*A. thaliana*	Reference
Spo11 catalytic core complex				(Arora et al., 2004; Kee et al., 2004)
Spo11	Rec12	SPO11	AtSPO11	(Bergerat et al., 1997; Grelon et al., 2001)
Ski8	Rec14		VIP3*	(Evans et al., 1997; Jolivet et al., 2006)
Rec102	Rec6	TOPOVIBL	MTOPVIB	(Robert et al., 2016; Vrielynck et al., 2016)
Rec104				
RMM complex				(Arora et al., 2004)
Rec114	Rec7	REC114	PHS1*	(Kumar et al., 2010)
Mei4	Rec24	MEI4	AtPRD2	(Kumar et al., 2010)
Mer2	Rec15	IHO1	AtPRD3	(Stanzione et al., 2016; Tessé et al., 2017)
MRX complex **				(Borde and Cobb, 2009; Furuse et al., 1998; Usui et al., 1998)
Mre11	Rad32	MRE11	MRE11	
Rad50	Rad50	RAD50	RAD50	
Xrs2	Nbs1	NBS1	NBS1	
Unclassified				
		MEI1	AtPRD1	(Libby et al., 2003; De Muyt et al., 2007)
	Mde2***			(Gregan et al., 2005; Miyoshi et al., 2012)
			DFO	
Axial Components ****				(Daniel et al., 2011; Ellermeier and Smith, 2005; Mao-Draayer et al., 1996; Sanchez-Moran et al., 2007; Xu et al., 2005)
Hop1	Hop1	HORMAD1/2	ASY1/2	(Rosenberg and Corbett, 2015)
Red1	Rec10	SYCP2?	ASY3?	(Ferdous et al., 2012; Lorenz, 2004; Offenberg et al., 1998)
Rec8	Rec8	Rec8/Rad21L	DIF1	(Bhatt et al., 1999; Ishiguro et al., 2011; Klein et al., 1999; Lee and Hirano, 2011; Parisi et al., 1999)

* Not essential for DSB formation.

** Essential for DSB formation in *S. cerevisiae*, but not in *S. pombe* and *A. thaliana*. The mammalian counterpart has not been identified.

*** Mde2 Interacts with Rec14 and Rec15.

**** Most of them are not essential for DSB formation, except for *S. pombe* Rec10.

Components in red boxes are orthologues or functional homologs of fission yeast Rec15, Hop1, and Rec10, which are of concern in this thesis.

2. Materials and methods

Medium

SD (without uracil)

Yeast nitrogen base (without amino acids)	6.7g
Glucose	20g
Agar	20g
Adenine, Leucine and Histidine	200mg each
Water	1L

SD (+5-FOA)

Yeast nitrogen base (without amino acids)	6.7g
Glucose	20g
Agar	20g
Adenine, Leucine and Histidine	200mg each
Uracil	100mg
5-Fluoroorotic acid (5-FOA)	800mg
Water	1L

CSM (without leucin, tryptophan, histidine, and adenine)

Following compounds were mixed;

2g Arginine HCl, 2g Isoleucine, 2g Lysine HCl, 2g Methionine, 3g Phenylalanine, 2g Serine, 2g Threonine, 2g Tyrosine,1.2g Uracil, and 9g Valine

SD (without leucin, tryptophan, histidine, and adenine)

Yeast nitrogen base (without amino acids)	6.7g
Glucose	20g
Agar	20g
CSM (without leucin, tryptophan, histidine, and Adenine)	600mg
Water	1L

SD (without leucin and tryptophan)

Yeast nitrogen base (without amino acids)	6.7g
Glucose	20g
Agar	20g
CSM (without leucin, tryptophan, histidine, and Adenine)	600mg
Adenine and Histidine	200mg each
RO Water	1L

SD (+10mM 3-AT without leucine, tryptophan, histidine and adenine)

Yeast nitrogen base (without amino acids)	6.7g
Glucose	20g
Agar	20g
CSM (without leucin, tryptophan, histidine, and Adenine)	600mg
Water	1L

final 10mM 3-Amino-1,2,4-triazole (3-AT) were added after autoclave

YES

Yeast extract	5g
Glucose	20g
Adenine, Leucine and Histidine	200mg each
Uracil	100mg
Agar	20g
Water	1L

YES (+Bsd)

Add Blasticidin S 100mg in 1L of YES after autoclave

YES (+Clonnat)

Add Clonnat 100mg in 1L of YES after autoclave

Salts

MgCl2・6H2O	52.5g
CaCl2・2H2O	0.735g
KCl	50g
Na_2SO4	2g
Water	1L

Vitamins

Calcium pantothenic acid	100mg
Nicotinic acid	100mg
myo-inositol	1g
Biotin	10mg
Water	100mL

Minerals

H_3BO_3	5g
$MnSO_4$	4g
$ZnSO_4・7H_2O$	4g
$FeCl_2・6H_2O$	2g
Molybdic acid	0.4g
KI	1g
$CuSO_4・5H_2O$	0.4g
Citric acid	10g
Water	1L

EMM2+Nitrogen (liquid)

Potassium Hydrogen Phthalate	3g
Na_2HPO_4	2.2
Glucose	20g
Salts	20mL
Vitamins	1mL
Minerals	100µl
NH_4Cl	5g
Water	1L

EMM-Nitrogen (liquid)

Potassium Hydrogen Phthalate	3g
Na_2HPO_4	2.2g
Glucose	10g
Vitamins	1mL
Salts	20mL
Minerals	100µL
Water	1L

EMM without leucine and histidine

EMM2+Nitrogen	1L
adenine	200mg
uracil	100mg
Agar	20g

EMM without adenine

EMM2+Nitrogen	1L
leucine and histidine	200mg each
uracil	100mg
Agar	20g

SPA

Glucose	20g
KH_2PO_4	1g
Vitamins	1mL
adenine	10mg
Agar	30g
Water	1L

Buffers

PBS

137mM NaCl, 8.1mM Na_2HPO_4, 2.68mM KCl, 1.47mM KH_2PO_4

ChIP lysis 140 buffer

0.1% Na-deoxycholate, 1mM EDTA, 50mM HEPES-KOH (pH 7.5), 140mM NaCl, 1% Triton X-100

ChIP lysis 500 buffer

0.1% Na-deoxycholate, 1mM EDTA, 50mM HEPES-KOH (pH 7.5), 500mM NaCl, 1% Triton X-100

ChIP wash buffer

0.5% Na-deoxycholate, 1mM EDTA, 10mM Tris-HCl (pH 8.0), 250mM LiCl, 0.5% NP-40

ChIP elution buffer

20mM Tris-HCl (pH8.0), 100mM NaCl, 20mM EDTA, 0.1% SDS

x1 TAE

40 mM Tris, 40mM Acetic acid, 1mM EDTA

ImmunoPrecipitation buffer

25mM MOPS-KOH (pH 7.2), 5mM EDTA, 0.1% NP-40, 150mM KCl, 1mM Dithiothreitol, 10% Glycerol

SDS sample buffer

125mM Tris-HCl (pH 6.8), 20% Glycerol, 4% SDS, 2% β-Mercaptoethanol, 0.001% Bromophenol blue

CSE buffer

20mM Citrate-phosphate (pH5.6), 1.2 M Sorbitol, 40mM EDTA (pH 8.0)

PFGE-TSE buffer

10mM Tris-Cl (pH 7.5), 0.9M Sorbitol, 45mM EDTA

PFGE-SDS buffer

0.25M EDTA (pH 8.0) 50mM Tris-Cl (pH 7.5) 5ml 1% SDS

PFGE-Sarcosine buffer

1% N-lauryl sarcosine 0.5 M EDTA (pH 9.5)

PEMS

100mM PIPES (pH 6.8), 1mM EGTA 1mM $MgSO_4$, 0.6M Sorbitol

Yeast strains and plasmid construction

Plasmids and strains used in this paper are listed in Tables 2 and 3. Point mutations were introduced by PCR-based site-directed mutagenesis using PrimeSTAR Max (Takara Bio, Shiga, Japan). For the deletion of *hop1*$^{+}$ gene, DNA fragments in which the *bsd*^{R} (Blastsidine resistant) marker cassette and *ura4*$^{+}$ gene cassette were flanked by an upstream and downstream sequences of *hop1*$^{+}$ were constructed by PCR amplification. This cassette DNA was transformed into yeast, and *hop1* disruptants were selected on YES medium containing Blastsidine (YES +Bsd) plates for *bsd*^{R}-harboring disruption mutants and on SD (without uracil) medium plate for *ura4*$^{+}$-containing disruption mutants. To obtain a point mutation in *rec10*$^{+}$ or *hop1*$^{+}$, each mutated gene fragment was transformed into a strain in which original *rec10*$^{+}$ or *hop1*$^{+}$ loci was replaced by *ura4*$^{+}$ marker gene, followed by selection on SD (+5-FOA) medium. Strains expressing epitope-tagged Hop1 were generated by integration of linearized pNATs plasmid with tagged-version of *hop1*$^{+}$ gene into *hop1* deletion strain. The pNAT plasmids containing epitope-tagged Hop1 were integrated into adjacent locus to *zfs1*$^{+}$ gene on chromosome 2. Mutants with intorsion were selected on YES (+Clonnat) medium plates.

Yeast two-hybrid assays and yeast three-hybrid assays

S. cerevisiae AH109 strain (Clontech, Mountain View, California) were transformed with pGADT7 and pGBKT7 plasmids harboring indicated bait and prey genes and selected on SD without leucine (L) and tryptophan (W) (SD w/o LW). Colonies were streaked on SD w/o LW, and further selected on SD medium without leucine, tryptophan, histidine (H) and adenine (A) (SD w/o LWAH). Cells were grown for 5 days at 30˚C, and their growth was analyzed on SD w/o LWAH to investigate interaction between bait and prey proteins.

For yeast three-hybrid assay, *S. cerevisiae* Y190 strain were transformed with pGADT7 and pGBKT7 plasmids and selected on SD w/o LW. Then transformants were sequentially transformed with pAde1 plasmids harboring ORF of wild type Hop1 gene, Hop1-9A or empty vector and selected on SD without leucine, tryptophan, and adenine (SD w/o LWA). Colonies were streaked on SD w/o LWA and further selected on SD w/o LWAH + 10mM 3-AT. Cells were grown for 5 days at 30˚C, and their growth was analyzed on SD w/o LWAH+ 10mM 3-AT to investigate the bridging by Hop1 between bait Rec10 and prey Rec15.

Culture and synchronized meiotic induction and cell fixation for ChIP

S. pombe culture and synchronous induction of meiosis were as described (Miyoshi et al., 2012). Briefly, the *pat1-114* mutant strains were cultured in EMM2 + nitrogen medium supplemented with adenine, leucine, histidine (200mg/L each) and uracil (100mg/L) at 25˚C. The culture was harvested, washed and re-suspended in EMM - nitrogen, then starved for 18 hours at 25˚C to arrest cells in G1 phase. The G1-arrested culture was transferred to EMM supplemented with amino acids (adenine, leucine, histidine and uracil) and low level of nitrogen (0.05% NH_4Cl) at 34˚C to induce synchronous meiosis. Cells were fixed as follow; 40 mL culture at density of 2 x 10^7 cells/mL was incubated at room temperature for 15 minutes after adding 1.1 mL of 37% formaldehyde (final concentration 1%). Fixation was terminated by adding 2.5 mL of 2 M glycine and cells were frozen in liquid nitrogen after washing with ice-chilled PBS.

ChIP experiments

ChIP assays were conducted as described previously (Hirota et al., 2007) with minor modification. Crosslinked cells were mixed with 500µl of zirconia beads and 300µl of ChIP lysis 140 buffer (supplemented with cOmplete

Protease Inhibitor Cocktail (Roche) and 1mM PMSF). Then cells were disrupted at 4˚C by Multibeads Shocker (Yasuikikai, Osaka, Japan) with 15 cycles of 2,500 rpm beating for 30 seconds and 1 minute interval. After disruption, the suspensions were sonicated six times on ice for 30 seconds each by handy sonic UR-20P (TOMY) and centrifuged at 17,500 x g for 5 minutes and supernatant were collected. Concentrations of lysate were measured by Bradford assay kit (BioRad, Hercules, California) and diluted equivalent to 4mg/mL of BSA.

Cell lysates were subjected to immunoprecipitation using antibodies described as follow. For FLAG-tagged Hop1, Rec15 and Rec10, anti-FLAG M2 antibody (SIGMA-Aldrich, St. Louis, Missouri) was incubated with ProteinA-dynabeads® (Thermo Fisher Scientific, Waltham, Massachusetts) and then added to cell lysates. For Rec8 and control IgG ChIP experiments, anti-Rec8 polyclonal antibody (Kitajima 2003) and rabbit IgG (Santa-cruz, Dallas, Texas) were added to the cell lysates followed by incubation and addition of ProteinA-sepharose (GE Healthcare, Chicago, Illinois). After 3 hours incubation with antibody at 4˚C, beads were washed twice by lysis140 buffer, once in lysis500 buffer and twice in wash buffer. Finally, beads were washed in TE. Bead-bound proteins and DNAs were then eluted by 100µl of ChIP elution buffer. Eluted protein and DNA were de-crosslinked by incubation at 75˚C over night and protein was digested by 10µg/mL proteinase K at 55˚C for 3 hours. After digestion, DNA was purified by FastGene Gel/PCR Extraction Kit (Nippon genetics, Tokyo, Japan). Purified DNA solution were used for qPCR assay and ChIP-sequencing analyses. qPCR was performed with KAPA SYBR FAST qPCR Kit (KAPA Biosystems) and StepOne Real-Time PCR system (Applied Biosystems). Primers used for qPCR are listed in Table 4. All buffers used are listed on p.20.

Data deposition of ChIP-sequencing

The ChIP-sequencing data is available at DDBJ (http://www.ddbj.nig.ac.jp) under accession number DRA007562.

ChIP-sequencing and peak calling

Library was prepared with NEBNext ChIP-Seq Library Prep Master Mix Set for Illumina (P/N E6240S, NEB, Ipswich, Massachusetts, United States) and NEBNext Multiplex Oligos for Illumina (P/N E7335S, NEB). Multiplexed libraries for ChIP-seq except for Rec8 ChIP were paired-end sequenced by MiSeq (MiSeq Reagent Kit v3; Illumina). Libraries for Rec8 ChIP, control IgG ChIP and Input were single-end sequenced. Reads were mapped to the *S.pombe* 972 *h*$^{-}$ genome sequence (AS294v230) using Bowtie2.

Peak detection was performed with MACS2 callpeak with options of "-nomodel –extsize 200 –broad –broad-cutoff 0.05".

For further analysis, we designated the 603 hotspots denoted by a previous study (Fowler et al., 2013) were designated as “DSB hotspots”. We defined LinE sites (also referred to as “Axis sites”) as Rec10 sites which does not overlap with DSB hotspot region with its fraction of greater than 20%. We excluded centromeric, telomeric and ribosomal DNA region from analysis. For the visualization of each ChIP-sequence data, the IP scores were divided by that of Input, normalized so that the median of log2 score is 0, and plotted every 25 bp with 250 bp window size. The software used is listed in Supplementary Table 5.

Co- immunoprecipitation

Co-IP was conducted as in previous research (Miyoshi et al., 2012). In detail, cells were mixed with 200μL of ImmunoPrecipitation buffer (see p.20) supplemented with cOmplete Protease Inhibitor Cocktail (Roche) and 1mM PMSF. Then 500μL of zirconia beads were added, and disrupted by Multibeads Shocker, with 5 cycles of 2,500 rpm beating for 30 seconds and 1 minute intervals on ice. Cell lysate were centrifuged at 13,000 x g for 10 minutes and supernatant were collected. Supernatant were mixed with anti-FLAG M2 affinity gel (SIGMA) and rotated for 2 hours at 4˚C. Then beads were washed 4 times in ImmunoPrecipitation buffer and boiled in SDS sample buffer.

Cross-linked Co- immunoprecipitation

Cross-linked Co-IP was conducted as in the previous research (Miyoshi et al., 2012). In detail, cells were fixed and frozen as in ChIP assay. Frozen cells were mixed with 200μL of lysis140 buffer (supplemented with 3mM $CaCl_2$ and 2.5U/mL MNase (Takara), cOmplete Protease Inhibitor Cocktail (Roche) and 1mM PMSF) and 500μL of zirconia beads, and then disrupted at 4˚C by Multibeads Shocker, with 5 cycles of 2,500rpm beating for 30 seconds and 1minute interval. After disruption, the suspensions were sonicated six times on ice for 30 seconds each by handy sonic UR-20P (TOMY) and centrifuged at 17,500 xg for 5 minutes and supernatant were collected. Supernatants were mixed with anti-FLAG M2 affinity gel (SIGMA) and rotated for 2 hours at 4˚C. Then beads were washed 4 times in lysis 140 buffer and boiled in SDS sample buffer.

Immunoblotting analysis

Anti-FLAG M2 antibody (Sigma-Aldrich), anti-HA 3F10 (Sigma-Aldrich) antibody were used as primary antibodies at dilution of 1 : 2,000, and anti-mouse IgG-HRP (GE Healthcare) and anti-rat IgG-HRP SC-2006 (Santa-cruz) were used as secondary antibodies at 1 : 2,000 dilution.

Prediction of protein structure by JPred4 and Phre2 server

The Rec10 N-terminal (201-400) protein structure was predicted using the PHYRE2 Protein Fold Recognition server (Protein Homology/analogY Recognition Engine V 2.0; http://www.sbg.bio.ic.ac.uk/phyre2/) (Kelley et al., 2015) to gain the predicted protein structure. The PHYRE2 program revealed that the N-terminal structure was similar to a domain called the C-lobe in the erythroid membrane protein 4.1r with 79.9% confidence. The C-lobe of erythroid membrane protein 4.1r is known to have a binding surface to the p55 protein (Han et al., 2000). Based on this biding surface residue information, residues of the biding surface in Rec10 were predicted and mutagenesis was carried out as described previously. Secondary structure predictions of Rec10 orthologues (*S.pombe* Rec10: Uniprot ID Q09823, *S.cerevisiae* Red1: Uniprot ID P14291, *M.musculus* SYCP2 : Uniprot ID Q9CUU3) were obtained using JPred4 (Drozdetskiy et al., 2015) (http://www.compbio.dundee.ac.uk/jpred/).

Pulsed field gel electrophoresis (PFGE) and Southern blotting

PFGE experiments were conducted as described previously (Cervantes et al., 2000). For plug preparation, cells were collected and washed twice in CSE buffer and cell wall were digested by 0.3mg/mL Zymolyase in PFGE-CSE for 1 hour at 37˚C. Then cells were collected and suspended in PFGE-TSE buffer so that cell concentration was $6x10^7$ cells/mL, mixed with 1% incert agarose (CAMBREX) dissolved in TSE and mold into plug. The plugs were soaked in PFGE-SDS buffer for 1.5 hours at 55˚C, then washed in PFGE-sarcosine buffer and incubated in PFGE-sarcosine buffer supplemented with 1mg/mL Proteinase K (Wako) for 48 hours at 55˚C.

For electrophoresis, plugs were embedded and separated in 0.8% agarose (Pulsed-field certified, BioRad) gel in x1 TAE at 14˚C for 24 hours. Conditions for PFGE with CHEF Mapper (BioRad) were: included angle, 106˚; initial switching time, 20 minutes; final switching time, 30 minutes. Gels were stained with x10,000 diluted SYBR® GreenI (Lonza, Basel, Switzerland) for 1 hour and the gel image was captured by ImageQuant LAS 4000 (GE Healthcare). All buffers used are listed on p.20.

Recombination assay

Mating and sporulation of haploid cells were conducted as previously described with minor modifications (Hirota et al., 2008). In brief, each yeast strain was cultured at 30˚C for overnight in YEA, harvested, and washed in 2 g/L of leucine. Then h^+ and h^- strains were combined and resuspended in a solution containing 1 g/L leucine, and 1 g/L histidine, followed by spotting on SPA plates. After two-day incubation on SPA at 30˚C, cells were digested in 0.5% glusulase (PerkinElmer, Waltham, Massachusetts) for 3 hours to isolate spores. For the

measurement of *leu1 – his5* intergenic recombination frequency, approximately 1,000 spores were inoculated on YEA plates and grown at 30˚C for 3 days. Grown colonies were counted, and spore viability was estimated as (the number of colonies grown on YEA) / 1,000. To measure *ade6-M26* x *ade6-469* intra-genic recombination frequency, 1×10^4 spores were inoculated on YEA plates followed by incubation at 30˚C for 2 days so that actual numbers of viable colony were [spore viability × 10,000], then replica-plated on EMM2 without adenine (EMM2-A). The intra-genic recombination frequency of *ade6* was calculated as (number of colonies grown on EMM2-A) / (spore viability × 10,000).

Microscopic observation

Haploid cells were grown on YEA plate overnight at 30˚C and then spotted on SPA plates to induce meiosis. 6 hours after incubation at 30˚C, the cells were fixed with methanol overnight at -20˚C and then stained by 1μg/ml of 4',6-diamidino-2-phenylindole (DAPI). Cells were re-suspended and washed with PEMS and observed by fluorescent microscopy.

Table 2 Plasmids used in this study

#1	pGADT7-Hop1 (Full Length)	*1
#2	pGADT7-Hop1 N (1-300aa)	*1
#3	pGADT7-Hop1 C (301-528aa)	*1
#4	pGADT7-Hop1 (9A-mutant)	Mutagenesis from #1
#5	pGADT7-Rec15 (Full Length)	*1
#6	pGADT7-Rec15 ΔCT (1-160aa)	Mutagenesis from #5
#7	pGADT7-Rec25 (Full Length)	*2
#8	pGBKT7-Hop1	*1
#9	pGBKT7-Rec15	*2
#10	pGBKT7-Mde2	*2
#11	pGBKT7-Rec10 (Full Length)	*2
#12	pGBKT7-Rec10 (291-791aa)	*2
#13	pGBKT7-Rec10 (449-791aa)	*2
#14	pGBKT7-Rec10 (1-651aa)	*2
#15	pGBKT7-Rec10 (1-496aa)	*2
#16	pGBKT7-Rec10 (1-348aa)	*2
#17	pGBKT7-Rec10 (1-193aa)	*2
#18	pGBKT7-Rec10 (E309A)	Mutagenesis from #11
#19	pGBKT7-Rec10 (P348G K349G)	Mutagenesis from #11
#20	NATZ-Phop1-Hop1-Thop1	
#21	NATZ-Phop1-Hop1-FLAG-Thop1	FLAG insertion to #20
#22	NATZ-Phop1-Hop1(9A-mutant)-FLAG-Thop1	Mutagenesis from #21
#23	NATZ-Phop1-Hop1-HA-Thop1	HA insertion to #20
#24	Rec15-FLAG-kan	*2
#25	Rec15ΔCT(1-160aa)-FLAG-kan	Mutagenesis from #24
#26	Rec10-FLAG-kan	*2
#27	Rec10(E309A)-FLAG-kan	Mutagenesis from #26
#28	Rec10(P348G K349G)-FLAG-kan	Mutagenesis from #26
#29	Rec10-GFP-ura4	*2
#30	Rec10(E309A)-GFP-ura4	Mutagenesis from #29
#31	Rec10(P348G K349G)-GFP-ura4	Mutagenesis from #29

*1 Plasmid used in Sakuno and Watanabe 2015 *2 Plasmid used in Miyoshi et.al., 2012

Table 3 Strains used in this study

Figure	Strain	Genotype	Source
3-8	YZ980	*h⁻ pat1-114 hop1⁺-GFP:kanMX6*	*1
	OTM416	*h⁻ pat1-114 ade6-M26 ura4-D18 rec15⁺-3FLAG:kanMX6 rec7⁺-3HA:ura4⁺*	*2
	OTM595	*h⁻ pat1-114 ade6-M26 ura4-D18 rec10⁺-3FLAG:kanMX6 rec7⁺-3HA:ura4⁺*	*2
	KR306	*h⁻ pat1-114 ade6-M26 ura4-D18 hop1:: ura4⁺ Z::P_{hop1}-hop1⁺-3FLAG-T_{hop1}-natʳ*	*1
10	KR98	*h⁻ pat1-114 ade6-M26*	*1
	KR306	*h⁻ pat1-114 ade6-M26 ura4-D18 hop1:: ura4⁺ Z::P_{hop1}-hop1⁺-3FLAG-T_{hop1}-natʳ*	*1
	KR308	*h⁻ pat1-114 ade6-M26 ura4-D18 rec10::hygʳ hop1:: ura4⁺ Z::P_{hop1}-hop1⁺-3FLAG-T_{hop1}-natʳ*	*1
	KR310	*h⁻ pat1-114 ade6-M26 ura4-D18 rec15::hygʳ hop1:: ura4⁺ Z::P_{hop1}-hop1⁺-3FLAG-T_{hop1}-natʳ*	*1
14A	KR224	*h⁻ pat1-114 ade6-M26 ura4-D18 hop1:: ura4⁺ Z::P_{hop1}-hop1⁺-3HA-T_{hop1}-natʳ*	*1
	KR229	*h⁻ pat1-114 ade6-M26 ura4-D18 rec10⁺-3FLAG:kanMX6 hop1:: ura4⁺ Z::P_{hop1}-hop1⁺-3HA-T_{hop1}-natʳ*	*1
14B	KR224	*h⁻ pat1-114 ade6-M26 ura4-D18 hop1:: ura4⁺ Z::P_{hop1}-hop1⁺-3HA-T_{hop1}-natʳ*	*1
	KR228	*h⁻ pat1-114 ade6-M26 ura4-D18 rec15⁺-3FLAG:kanMX6 hop1:: ura4⁺ Z::P_{hop1}-hop1⁺-3HA-T_{hop1}-natʳ*	*1
	KR231	*h⁻ pat1-114 ade6-M26 ura4-D18 rec15ΔCT(20aa)-3FLAG:kanMX6 hop1Δura4+ P_{hop1}-hop1⁺-HA-T_{hop1}- natʳ*	*1
15CD	KR98	*h⁻ pat1-114 ade6-M26*	*1
	KR306	*h⁻ pat1-114 ade6-M26 ura4-D18 hop1:: ura4⁺ Z::P_{hop1}-hop1⁺-3FLAG-T_{hop1}-natʳ*	*1
	KR307	*h⁻ pat1-114 ade6-M26 ura4-D18 hop1:: ura4⁺ Z::P_{hop1}-hop1-9A-3FLAG-T_{hop1}-natʳ*	*1
16	OTM557	*h- pat1-114 ade6-M26 ura4-D18 rec7+-3HA:ura4+*	*2
	OTM595	*h⁻ pat1-114 ade6-M26 ura4-D18 rec10⁺-3FLAG:kanMX6 rec7⁺-3HA:ura4⁺*	*2
	KR39	*h⁻ pat1-114 ade6-M26 ura4-D18 rec10⁺-3FLAG:kanMX6 rec7⁺-3HA:ura4⁺ hop1::bsdʳ*	*1
	OTM607	*h⁻ pat1-114 ade6-M26 ura4-D18 rec15::hygʳ rec10⁺-3FLAG:kanMX6 rec7⁺-3HA:ura4⁺*	*2
17	OTM557	*h- pat1-114 ade6-M26 ura4-D18 rec7+-3HA:ura4+*	*2
	OTM416	*h⁻ pat1-114 ade6-M26 ura4-D18 rec15⁺-3FLAG:kanMX6 rec7⁺-3HA:ura4⁺*	*2
	KR38	*h⁻ pat1-114 ade6-M26 ura4-D18 hop1::bsdʳ rec15⁺-3FLAG:kanMX6 rec7⁺-3HA:ura4⁺*	*1
	OTM578	*h⁻ pat1-114 ade6-M26 ura4-D18 rec10::hygʳ rec15⁺-3FLAG:kanMX6 rec7⁺-3HA:ura4⁺*	*2
	KR95	*h⁻ pat1-114 ade6-M26 ura4-D18 rec15ΔCT(20aa)-3FLAG:kanMX6 rec7⁺-3HA:ura4⁺*	*1

(continued on the next page)

Table 3 (continued)

Figure	Strain	Genotype	Source
18	KR98	*h⁻ pat1-114 ade6-M26*	*1
	KR100	*h- pat1-114 ade6-M26 ura4-D18 hop1:: ura4⁺*	*1
	KR155	*h- pat1-114 ade6-M26 hop1-9A*	*1
19BD	KR261	*h⁻ ade6-469 leu1-32*	*1
	KR262	*h⁺ ade6-M26 his5-303*	*1
	KR265	*h- ade6-469 leu1-32 hop1-9A*	*1
	KR266	*h⁺ ade6-M26 his5-303 hop1-9A*	*1
	KR25	*h⁻ ade6-469 ura4-D18 leu1-32 hop1:: ura4⁺*	*1
	KR28	*h⁺ ade6-M26 ura4-D18 his5-303 hop1:: ura4⁺*	*1
20	OTM595	*h⁻ pat1-114 ade6-M26 ura4-D18 rec10⁺-3FLAG:kanMX6 rec7⁺-3HA:ura4⁺*	*2
	KR39	*h⁻ pat1-114 ade6-M26 ura4-D18 rec10⁺-3FLAG:kanMX6 rec7⁺-3HA:ura4⁺ hop1::bsd^r*	*1
	OTM607	*h⁻ pat1-114 ade6-M26 ura4-D18 rec15::hyg^r rec10⁺-3FLAG:kanMX6 rec7⁺-3HA:ura4⁺*	*2
21	OTM416	*h⁻ pat1-114 ade6-M26 ura4-D18 rec15⁺-3FLAG:kanMX6 rec7⁺-3HA:ura4⁺*	*2
	KR38	*h⁻ pat1-114 ade6-M26 ura4-D18 hop1::bsd^r rec15⁺-3FLAG:kanMX6 rec7⁺-3HA:ura4⁺*	*1
	OTM578	*h⁻ pat1-114 ade6-M26 ura4-D18 rec10::hyg^r rec15⁺-3FLAG:kanMX6 rec7⁺-3HA:ura4⁺*	*2
23A	KR336	*h^{90} rec10⁺-GFP: ura4⁺*	*1
	KR337	*h^{90} rec10(P348G K349G)-GFP: ura4⁺*	*1
	KR338	*h^{90} rec10(E309A) -GFP: ura4⁺*	*1
23B	KR224	*h⁻ pat1-114 ade6-M26 ura4-D18 hop1:: ura4⁺ Z::P$_{hop1}$-hop1⁺-3HA-T$_{hop1}$-nat^r*	*1
	KR229	*h⁻ pat1-114 ade6-M26 ura4-D18 rec10⁺-3FLAG:kanMX6 hop1:: ura4⁺ Z::P$_{hop1}$-hop1⁺-3HA-T$_{hop1}$-nat^r*	*1
	KR407	*h⁻ pat1-114 ade6-M26 ura4-D18 rec10(E309A)-3FLAG:kanMX6 hop1:: ura4⁺ Z::P$_{hop1}$-hop1⁺-3FLAG-T$_{hop1}$-nat^r*	*1
	KR408	*h⁻ pat1-114 ade6-M26 ura4-D18 rec10(P438G K349G)-3FLAG:kanMX6 hop1:: ura4⁺ Z::P$_{hop1}$-hop1⁺-3FLAG-T$_{hop1}$-nat^r*	*1

(continued on the next page)

Table 3 (continued)

Figure	Strain	Genotype	Source
25	KR261	*h⁻ ade6-469 leu1-32*	*1
	KR262	*h⁺ ade6-M26 his5-303*	*1
	KR267	*h⁻ ade6-469 leu1-32 rec10(P348G K349G)*	*1
	KR268	*h⁺ ade6-M26 his5-303 rec10(P348G K349G)*	*1
	KR300	*h⁻ ade6-469 leu1-32 rec10(E309A)*	*1
	KR301	*h⁺ ade6-M26 his5-303 rec10(E309A)*	*1
	KR25	*h⁻ ade6-469 ura4-D18 leu1-32 hop1:: ura4⁺*	*1
	KR28	*h⁺ ade6-M26 ura4-D18 his5-303 hop1:: ura4⁺*	*1
	KR238	*h⁻ ade6-469 ura4-D18 leu1-32 rec10(P348G K349G) hop1:: ura4⁺*	*1
	KR239	*h⁺ ade6-M26 ura4-D18 his5-303 rec10(P348G K349G) hop1:: ura4⁺*	*1
	KR302	*h⁻ ade6-469 ura4-D18 leu1-32 rec10(E309A) hop1:: ura4⁺*	*1
	KR303	*h⁺ ade6-M26 ura4-D18 his5-303 rec10(E309A) hop1:: ura4⁺*	*1
	KR42	*h⁻ ade6-469 ura4-D18 leu1-32 rec10:: ura4⁺*	*1
	KR43	*h⁺ ade6-M26 ura4-D18 his5-303 rec10:: ura4⁺*	*1
	KR58	*h⁻ ade6-469 ura4-D18 leu1-32 rec15:: ura4⁺*	*1
	KR59	*h⁺ ade6-M26 ura4-D18 his5-303 rec15:: ura4⁺*	*1
	KR413	*h⁻ ade6-469 leu1-32 rec15(ΔCT20aa)*	*1
	KR414	*h⁺ ade6-M26 his5-303 rec15(ΔCT20aa)*	*1
26	KR98	*h⁻ pat1-114 ade6-M26*	*1
	KR100	*h- pat1-114 ade6-M26 ura4-D18 hop1:: ura4⁺*	*1
	KR343	*h- pat1-114 ade6-M26 rec10(P348G K349G)*	*1
	KR345	*h- pat1-114 ade6-M26 rec10(P348G K349G) hop1:: ura4*	
	KR344	*h- pat1-114 ade6-M26 rec10(E309A)*	*1
	KR346	*h- pat1-114 ade6-M26 ura4-D18 rec10(E309A) hop1:: ura4⁺*	*1
	KR354	*h⁻ pat1-114 ade6-M26 ura4-D18 rec10:: ura4⁺*	*1

*1 This study

*2 Miyoshi et. al., 2012

Table 4 Primers used in ChIP-qPCR assay

	Sites	Primer	Sequence
Axis	SPBC3H7.03c	CHIP_SPBC3H7.03c_F	TGCCATGAATTCCTATCGTAG
		CHIP_SPBC3H7.03c_R	GTTGCAAGGCTTATGTACATAC
	ura1-down	ChIP_ura1down__newF	TATCGTTATGCATCCTTTGC
		ChIP_ura1_down_newR	TTCAGTAGCACCCATAACAC
	sib1-down	ChIP_sib1_down_F	TGCACGATACTTGCTTGAAG
		ChIP_sib1_down_R	CATCCATCGTATAATGCATG
	SPCC594.01	ChIP_SPCC594.01_F	GACATACACTATAGATGCAG
		ChIP_SPCC594.01_R	GCTGTTCAATAGGCTTCTTG
DSB hotspot	mbs1	CHIP_mbs1_F	AAACACTGGTCATCTCGGAACCAGC
		CHIP_mbs1_R	TCCTTTGCAGTGAATGGTTGGGCTAC
	sat1	ChIP_sat1_F	TCATCTCATTAAGAGTGTTCGG
		ChIP_sat1_R	GATGCAAAGCAAATGCGCAAGT
	ste11	CHIP_ste11_F	TCATCTTTACCTCTACTTTC
		CHIP_ste11_R	ACAAGGTTGAGCTTAAAAGG
	mae2	ChIP_mae2_F	GTTGTAAAGATTGTTCTCGG
		ChIP_mae2_R	CTTTAAATGAATGATCCCCC
Cold Spot	sib1	ChIP_sib1_F	TGGCTCTAGATGTATCAGCG
		ChIP_sib1_R	ACGGCTGTCGAATCAGTTAC
	dis2	ChIP_dis2_F	TTGTTTTATTGAAGCTCCGC
		ChIP_dis2_R	ATTGTATGCCATTGAATCCC
	ime4	ChIP_ime4_F	TACAGTTTGAGGATCAGTGC
		ChIP_ime4_R	CCATCATTTTGGACACATTG

Table 5 Software used in this study

	Reference	Version
Bowtie2	(Langmead and Salzberg, 2012)	2.2.9
MACS2	(Zhang et al., 2008)	2.1.1
Integrative genomics viewer	(Robinson et al., 2011)	2.3.92
IGVtools	(Thorvaldsdóttir et al., 2013)	2.3.68
Bedtools	(Quinlan and Hall, 2010)	2.17.0

3. Results

Chapter 1: Genome wide analysis of Hop1

Genome wide analysis of axis meiotic chromosome in fission yeast

To gain insights into the function of Hop1, I first investigated the genome-wide distribution of fission yeast Hop1 by ChIP-seq analysis, in comparison with the previous mapping results of Rec12-oligo, which most precisely identified the position of DSB hotspots (Fowler et al., 2013) (Figure 3A bottom lane). I also carried out ChIP-seq assays of Rec8, Rec10, and Rec15 as references (Figure 3). The cultures were cross-linked and harvested during meiotic prophase, after cells had completed DNA replication. The synchronized cell cycle of haploid meiosis was monitored by flow cytometry analysis (Figure 4).

First, I determined chromosome axis sites form obtained ChIP-seq data. The counterpart of axis in fission yeast is Linear elements (LinEs), whose major component is Rec10. Previous study had defined the genomic region of LinEs, as Rec10 binding region outside of DSB hotspots determined from ChIP-chip data (Miyoshi et al., 2012; Yamada et al., 2018). Therefore, I redefined LinEs form ChIP-seq data of Rec10 and mapping results of Rec12-oligo. In detail, I detected 1,155 Rec10 binding sites (Figure 5A), in which 226 sites are overlapped with DSB hotspot region, 75 sites partially (less than 20% of Rec10 region) overlapped with DSB hotspot sites and 854 sites did not overlap with DSB hotspot region. I designated 854 non-DSB-overlapping Rec10 sites, and 75 partially-DSB-overlapping Rec10 sites as LinE region (also referred to as Axis stes)(Figure 5A and B). ChIP-seq data of Rec8 indicates Rec8 is enriched around LinE sites (Figure 5C top and D), supporting the speculation that Rec8 binding sites overlap with chromosome axis sites. I detected only a few overlaps of Rec8

peaks and DSB hotspots, as reported previously (Ito et al., 2014), (Figure 5C bottom): only 32 of the 999 Rec8 peaks overlapped with DSB hotspots.

Genome wide analysis of Hop1 localization

Then I examined Hop1 localization in relation to LinE sites and DSB hotspot sites. After peak calling, I detected 938 Hop1 peaks and compared them to the LinE sites ("axis sites") and the Rec12 oligo peaks ("DSB hotspots"). I observed that the majority of Hop1 peaks were colocalized with LinE sites (642 of 938 Hop1 peaks, 68.4%; Figure 6A left), indicating that Hop1 is mainly localized in the axis, consistent with the finding that 823 Hop1 peaks (87.7%) overlapped with the Rec10 binding sites (Figure 5B left). On the other hand, 226 of 938 Hop1 peaks (24.0%) overlapped with DSB hotspots (Figure 6A right). It should be noted that about half of the Hop1 sites (549 of 938 Hop1 peaks, 58.5%) coexisted with Rec15 binding sites (Figure 6B right).

The binding of Hop1 to both the axis and DSB hotspots was similar to that of Rec10 and Rec15 reported in the previous study (Miyoshi et al., 2012) (Figure 5A, Figure7 and Figure8). I therefore speculated that Hop1 may interact with Rec10 and Rec15. As such, I examined whether Hop1 distribution is affected in the deletion mutants for Rec10 or Rec15 by qPCR-based ChIP assay (Figure 10). In *rec10*Δ, Hop1 localization was not observed on neither the axes nor DSB hotspots, although this may be partly caused by reduced Hop1 amount or stability (Figure 10A and B). In the *rec15*Δ strain, Hop1 was retained in the axis but was no longer detected in the DSB hotspots (Figure 10B). Accordingly, Rec10 is a prerequisite for chromatin-binding of Hop1 and Rec15 is required for the DSB hotspot-binding of Hop1. This suggests that Hop1, which can interact with both

Rec15 and Rec10, is first loaded to the axis via Rec10 and eventually recruits DSB hotspot-bound Rec15. Consistent with this idea, Hop1 reportedly interacts with Rec10 (Estreicher et al., 2012; Spirek et al., 2010), and mouse Hop1 homolog HORMAD1 interacts with mouse Rec15 homolog IHO1 (Stanzione et al., 2016).

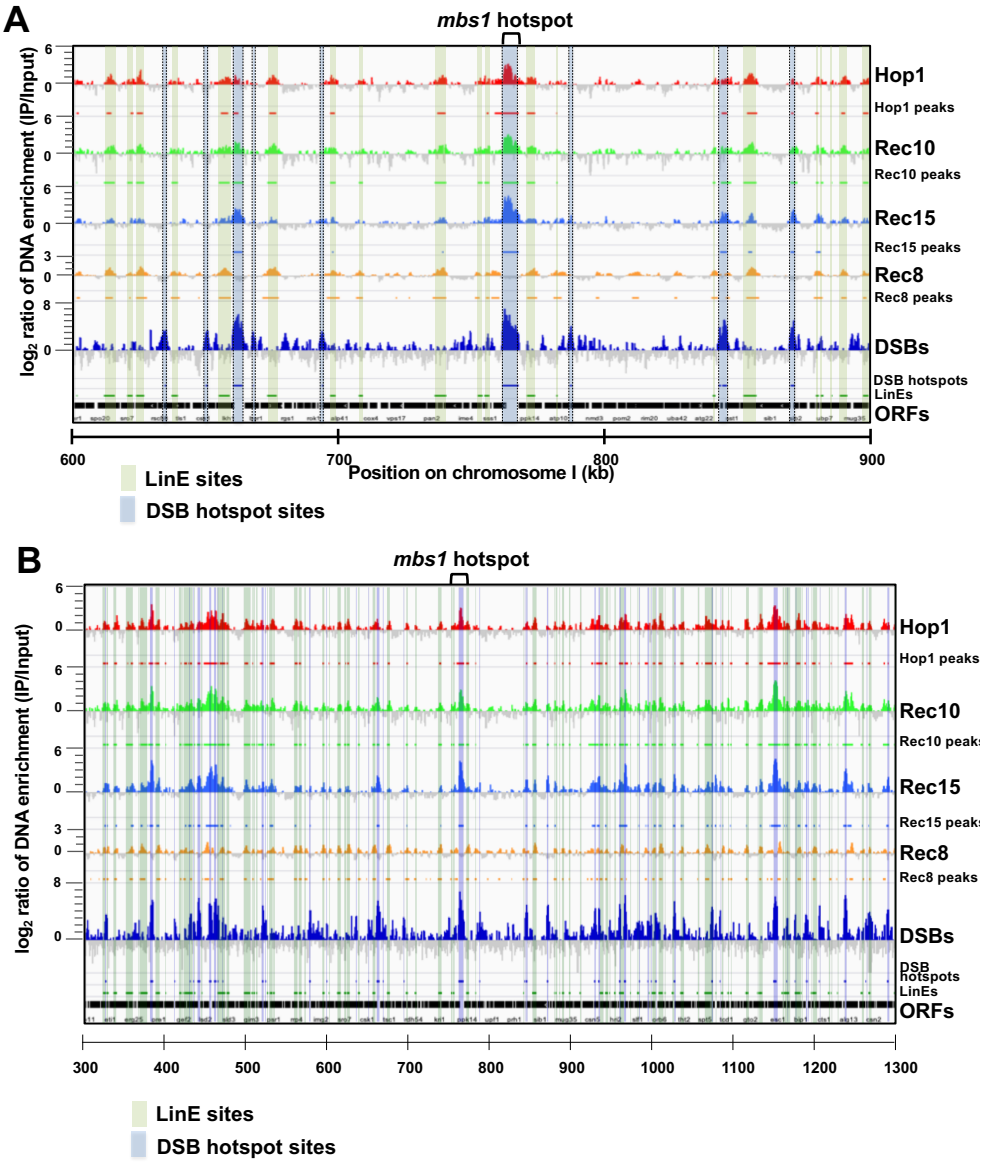

Figure 3

(A) ChIP-seq data of Rec8, Hop1, Rec10, and Rec15 around *mbs1* DSB hotspot locus. Cells were cross-linked and harvested at 4 hours after meiotic induction (for Hop1, Rec15, and Rec10 ChIP-seq) and at 3.5 hours (for Rec8 ChIP-seq). The Y-axis represents $\log_2$ scaled DNA enrichment (IP-read counts per Input-read counts). DSBs represents data of Rec12-oligo count from previous study (Fowler et al., 2013). Black horizontal bars at the bottom represent the open reading frames. A band with grey shading between two dotted lines indicates the region of the *mbs1* DSB hotspot and other DSB hotspots. Light green-shaded bands represent chromosome axis (LinE) sites. The DSB hotspot positions data are from a previous study (Fowler et al., 2013). (B) Wide range views of ChIP-seq data of Rec8, Hop1, Rec10, and Rec15 around *mbs1* DSB hotspot locus. Black bars at the bottom indicate the open reading frames.

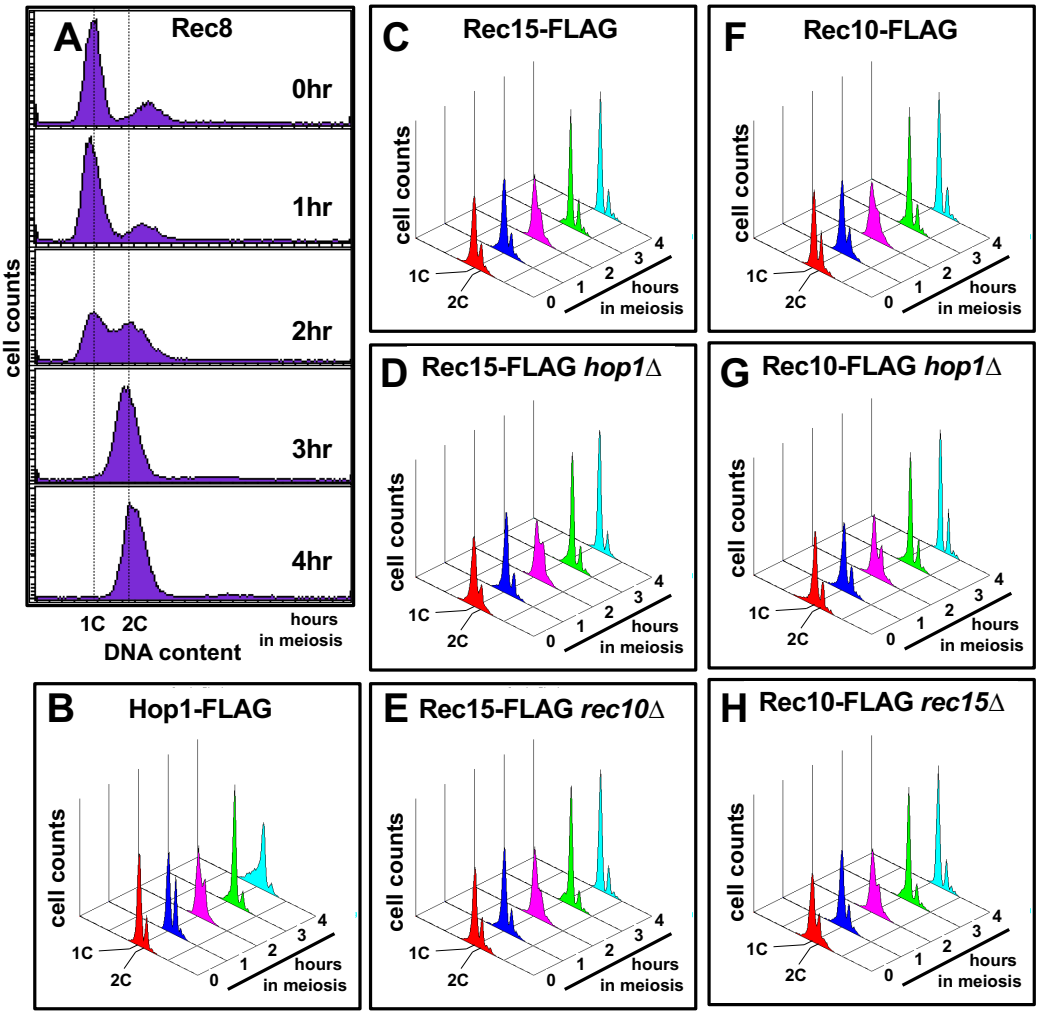

Figure 4

(A)-(H) Meiotic cell cycle analysis by flow cytometry

(A) Meiotic progression of cells used for Rec8 ChIP experiments. Y- and X-axes represent cell counts and DNA content, respectively. (B)-(H) Meiotic progression of cells expressing FLAG-tagged versions of Hop1, Rec10, and Rec15. Y- and X-axes represent the cell counts and DNA content, respectively. Z-axis indicates the time after meiotic induction.

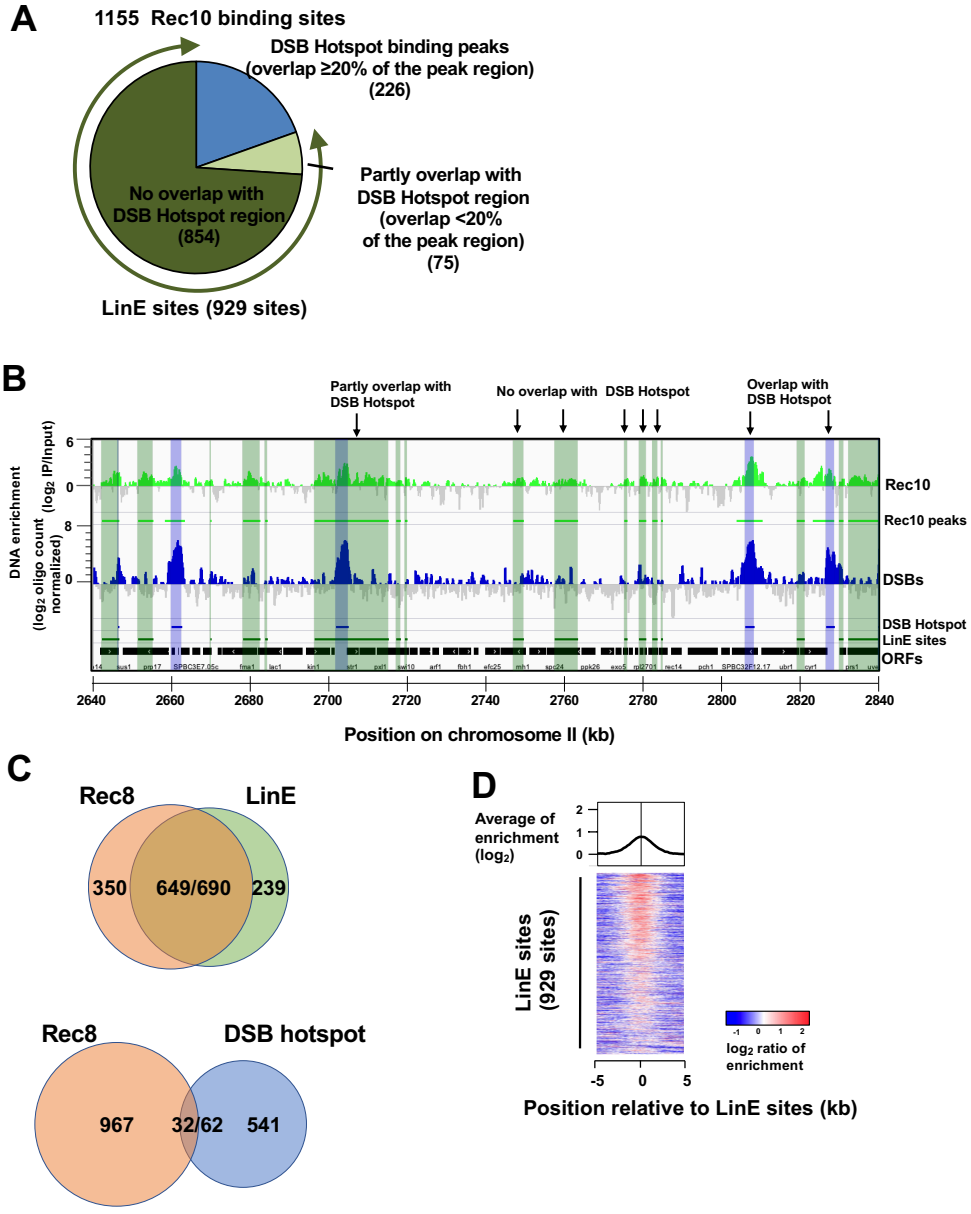

Figure 5

(A) A pie chart showing the classification of Rec10 peaks. Rec10 peaks overlapping with DSB hotspot sites with their fraction of greater than 20% are classified as DSB Hotspot binding peaks. Other Rec10 peaks are classified as LinE sites.(B) Examples of Rec10 peaks classified into LinE sites and DSB overlapping sites.(C) Venn diagrams showing the overlap between Rec8 binding sites and LinE sites (left), and between Rec8 binding sites and DSB hotspot sites (right). The numbers indicate the number of binding sites. In the left venn-diagram, two numbers separated by " / " in the intersection region (649/690) indicates 649 Rec8 binding sites overlap with 690 LinE sites. The discrepancy of peak count in intersection occurs because occasionally more than one LinE sites overlaps one Rec8 site. Likewise, in the right diagram (32/62) indicates 32 Rec8 binding sites overlap with 62 DSB hotspot sites. (D) Heat map images of ChIP-seq signals of Rec8 around LinE sites. LinE sites are sorted by Rec10 ChIP fold enrichments.

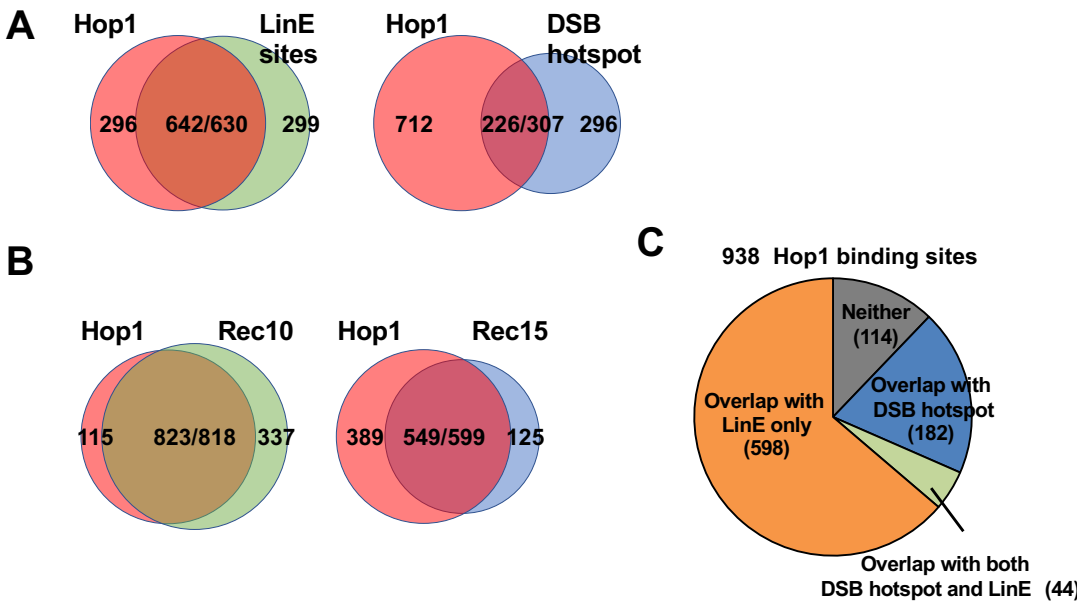

Figure 6

(A) Venn-diagrams showing the overlap between Hop1 sites and LinE sites (left), and between Hop1 sites and DSB hotspots (right). The numbers indicate the number of binding sites. For two numbers separated by " / " in the intersection region, refer Figure 5C. (B) Venn diagrams showing the overlap between Rec10 sites and Hop1 sites (left), Hop1 sites and Rec15 sites (right). The numbers in the diagrams indicate the number of each site. Two numbers separated by " / " in the intersection region are described in Figure 5C. (C) A pie chart of Hop1 peaks classified by overlapping status with LinE sites and/or DSB hotspots. The numbers in parenthesis represent the number of sites in each category.

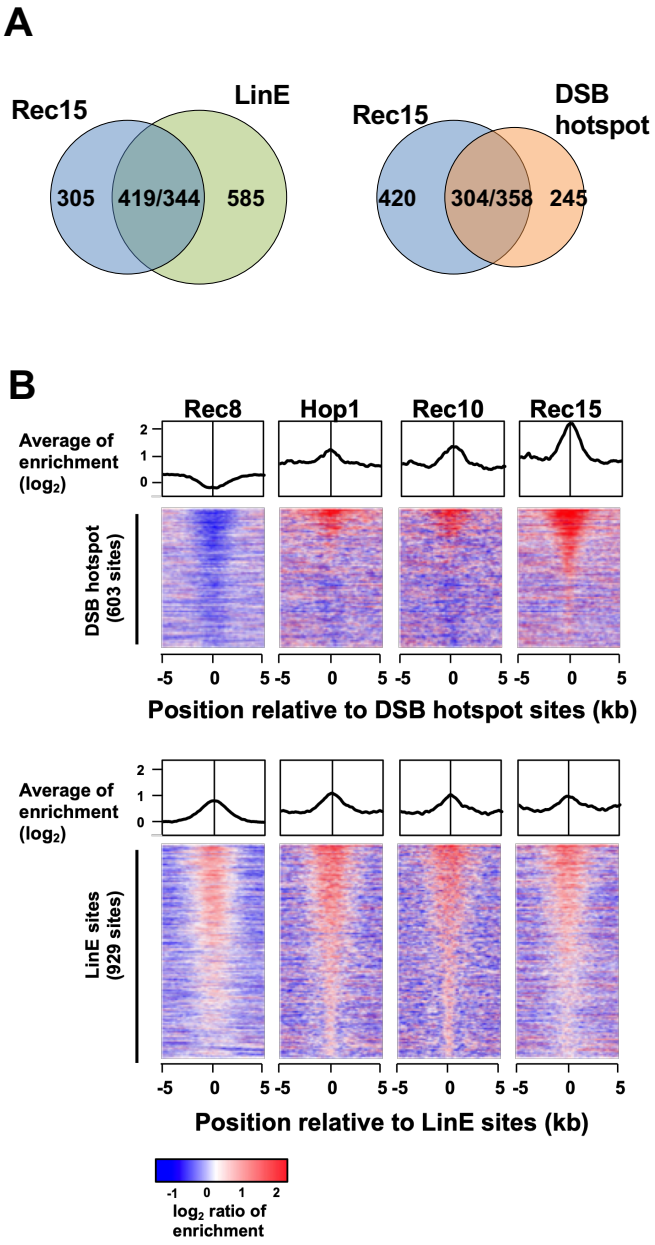

Figure 7

(A) Venn-diagrams showing the overlap between Rec15 and LinE sites (left) and between Rec15 and DSB hotspot sites (right). The numbers in the diagrams indicate the number of each site. For two numbers separated by " / " in the intersection region, refer Figure 5C.

(B) Heat map images of ChIP-seq signals of control (IgG), Rec8, Hop1, Rec10, and Rec15 around DSB hotspot sites and LinE sites. DSB hotspots are sorted by Rec12-oligo counts reported in the previous study (Fowler et al., 2013). LinE sites are sorted by Rec10 ChIP fold enrichments.

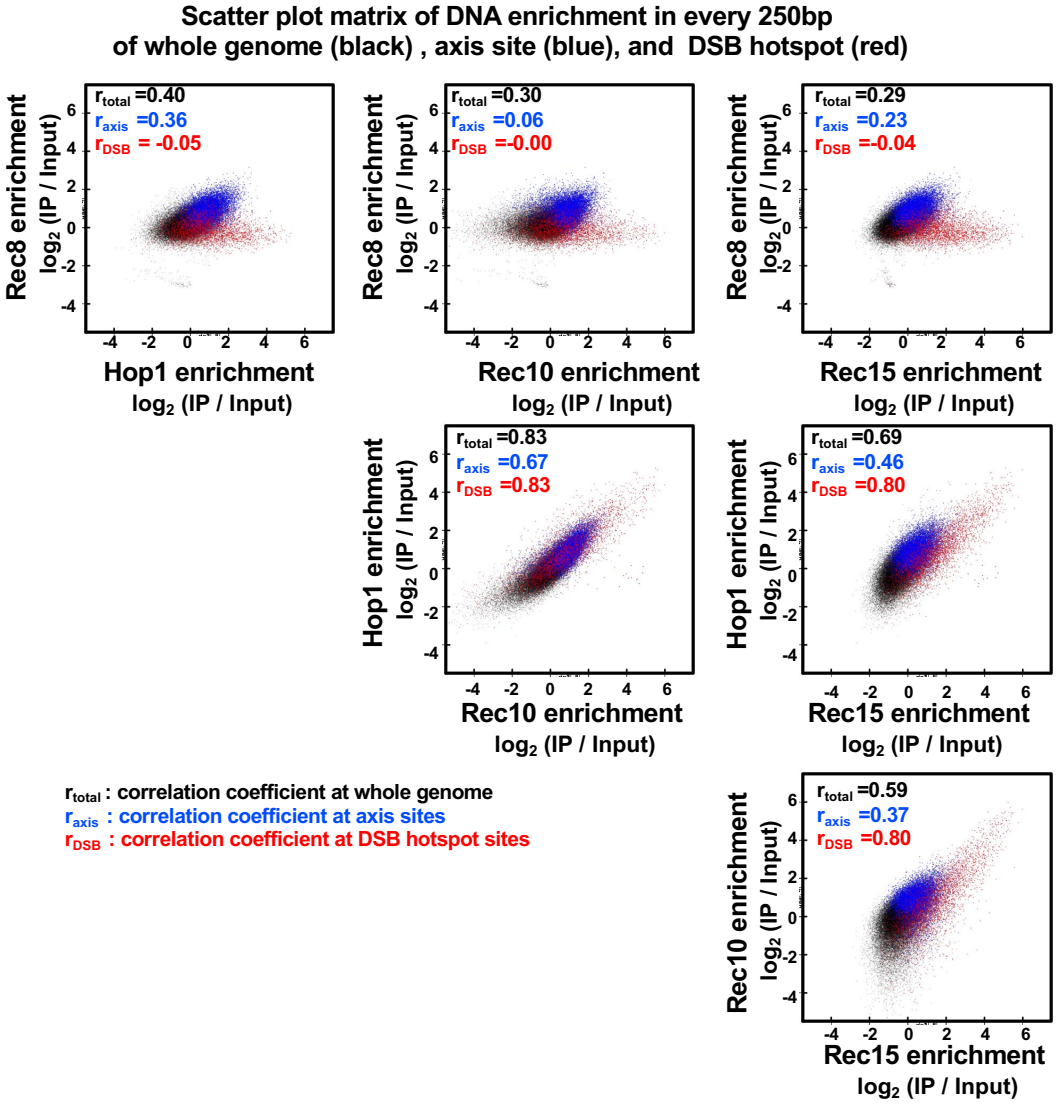

Figure 8

(A) Scatter plots of DNA enrichment (log2-scaled IP read counts/Input read counts) for two parameters indicated on the X- and Y-axis. Whole genome data points (250 bp each) except for the centromere region and the telomere region were plotted in black dots. Data points within aixs sites are indicated in blue dots. Data points within DSB hotspot regions are indicated in red dots. Values of r_{total} indicate Pearson correlation coefficients in whole genome data points, r_{axis} indicate Pearson correlation coefficients in axis sites, r_{DSB} indicate Pearson correlation coefficients in DSB hotspot sites.

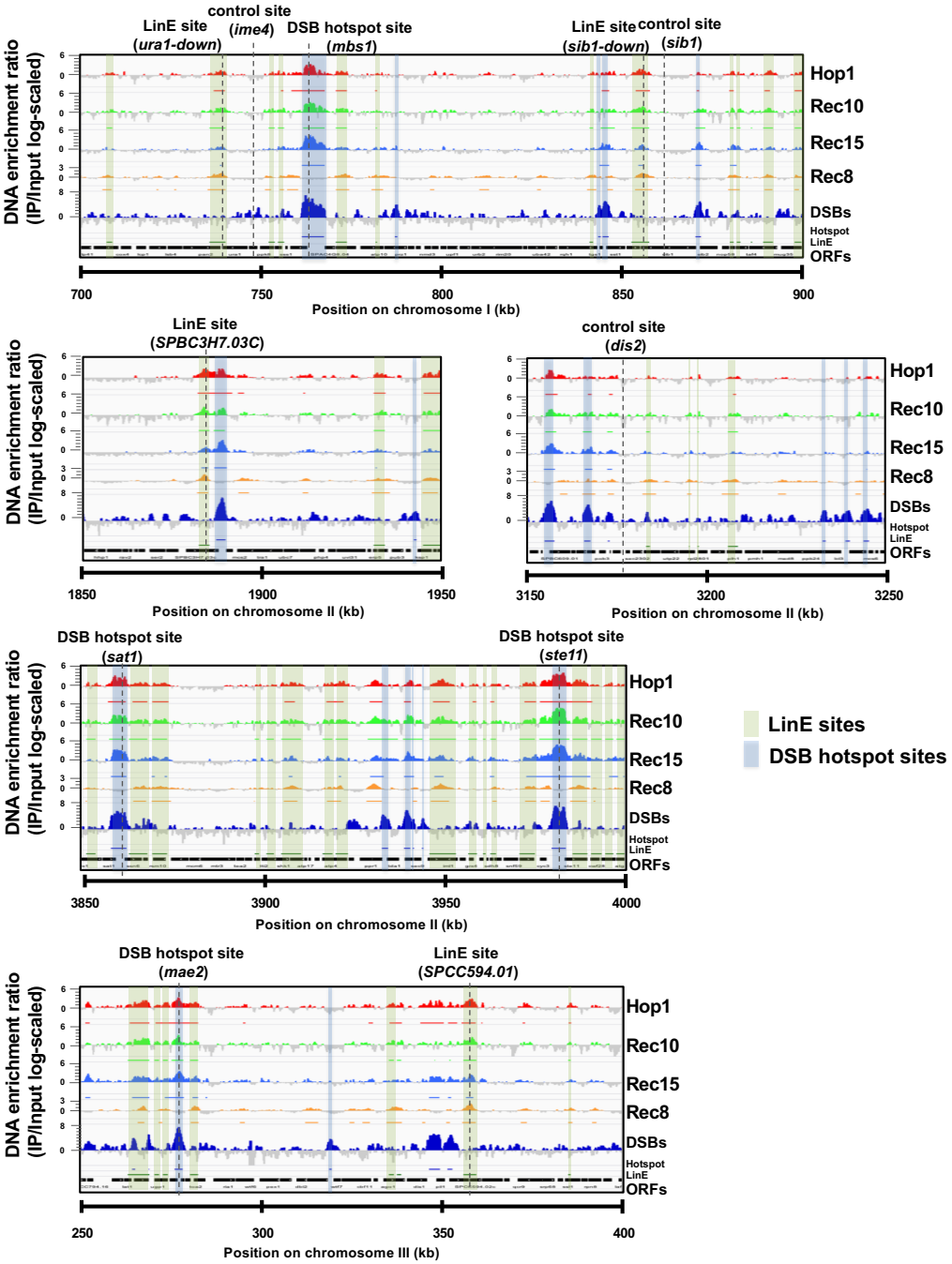

Figure 9

ChIP-seq data of Rec8, Hop1, Rec10, and Rec15, and Rec12 oligo count (DSBs) around Positions of ChIP-qPCR primers tested in this paper (axis; *SPBC3H7.03c, ura1-down, sib1-down, SPCC594.01,* DSB hotspot; *mbs1, sat1, mae2, and ste11*, and control sites; *dis2 ime4,* and *sib1*). The Y-axis represents log2-scaled DNA enrichment (IP read counts/Input read counts). Gray horizontal bars represent open reading flames. Count of Rec12 oligonucleotides are described in previous study. (Fowler et al. 2013) Vertical dotty lines indicates precise position of ChIP-qPCR primers.

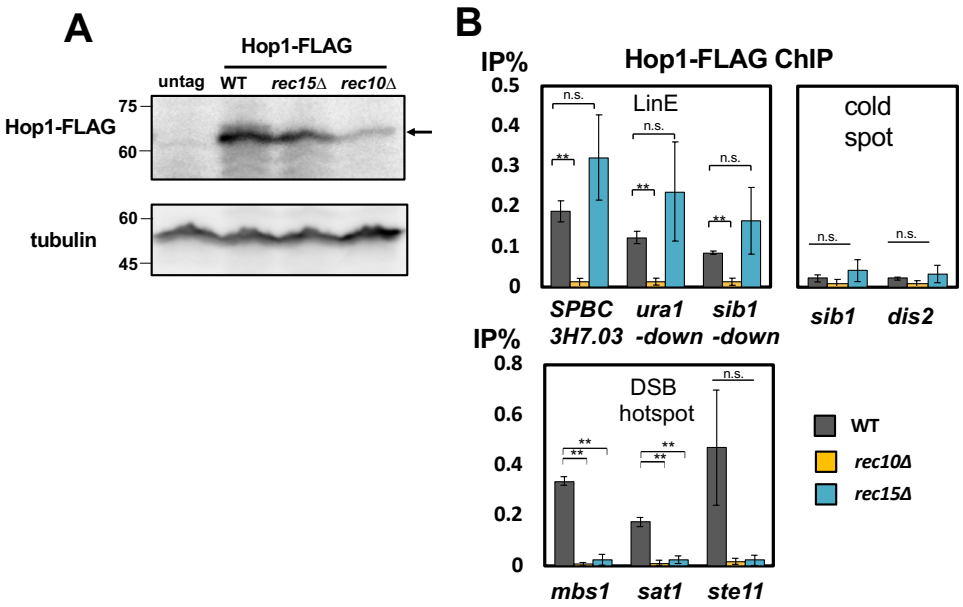

Figure 10

(A) Protein abundance of FLAG-tagged Hop1 in wild type, *rec15*Δ, and *rec10*Δ cells. Upper picture: anti-FLAG blotting. Lower picture: anti-tubulin blotting. An arrow indicates the position of Hop1-FLAG. (B) ChIP-qPCR analysis of Hop1 in the background of wild type, *rec15*Δ, and *rec10*Δ. Error-bars represent standard deviations of three biological replicates. q-PCR experiments were performed with the primer sets for detection of the LinE binding (LinE, *SPBC3H7.03c, ura1-down,* and *sib1-down*), DSB hotspot binding (DSB, *mbs1, sat1,* and *ste11*), and control sites (cold spot., *sib1* and *dis2*). The primer sets for qPCR are listed and described in Table 4 and Figure 9.

Chapter 2: Protein interaction of Hop1

Hop1 interacts with Rec15 and Rec10

Then I examined the interaction of Hop1 with Rec15 and Rec10 via yeast two-hybrid (Y2H) assays followed by domain analyses (Figure 11A and B). The Y2H assay results confirmed that the full-length and the N-terminal region of Hop1 (harbouring HORMA domain) interacted with Rec10, and that the C-terminal domain of Hop1 interacted with Rec15 (Figure 11B).

I also explored which Rec15 domains were required for its interaction with Rec10, Hop1, Mde2, and with Rec15 itself. Mde2 is another essential meiotic DSB protein which interacts with the Rec7-Rec15-Rec24 (SFT) and Rec12-containing catalytic (DSBC) subcomplexes (Figure 11A and C). Mde2 stabilizes the SFT subcomplex and recruits the DSBC subcomplex to DSB sites, depending on the DNA replication checkpoint (Miyoshi et al., 2012). Self-interaction of Rec15 is a common feature of Rec15 related proteins, though its significance is not known (Miyoshi et al., 2012; Stanzione et al., 2016; Tessé et al., 2017). Deletion of the conserved C-terminal segment of Rec15 (Tessé et al., 2017) (Rec15ΔCT, Figure 11 A, B and D) leads to a marked reduction in its interaction with both Hop1 and Rec10, though Rec15ΔCT retained binding to Mde2 and Rec15-Rec15 self-interaction (Figure 11D). Therefore, the Rec15 C-terminal domain is essential for binding to both Hop1 and Rec10, but not for Mde2 or Rec15 itself.

The previous study reported that Rec10 interacts with Rec15 and AE component Rec25 as well as Hop1 (Estreicher et al., 2012; Miyoshi et al., 2012). To narrow down the domain of Rec10 responsible for the interaction with Hop1, Rec15, and Rec25, I further divided Rec10 into several domains and surveyed their

interaction with Hop1, Rec15 and Rec25. Then I found that N-terminal region of Rec10 interacts with Rec15, the middle region of Rec10 is enough to bind to Hop1 and the C-terminal region of Rec10 interacts Rec25 (Figure 12).

To further narrow down the Hop1 residues responsible for the interaction with Rec15, I tested several point mutants of Hop1 via Y2H assay. Hop1 has PHD-like zinc finger domain in its C-terminal domain. The alanine scanning of zinc finger domain revealed that alanine substitution of several acidic residues in PHD-like zinc finger domain (#3, #4, #8 and #9 in Figure 13A) caused loss of the interaction with Rec15 but retained the interaction with Rec10. Those residues responsible for Rec15 binding presumably form acidic surface in the PHD domain (Figure 13B).

The interactions between Hop1-HA and Rec15-FLAG (full-length and ΔCT) or Rec10-FLAG was then tested by co-immunoprecipitation (co-IP) experiments. I detected Hop1-HA in the Rec10-FLAG immunoprecipitates (Figure 14A), confirming the interaction between Hop1 and Rec10. The interaction between the full-length Hop1-HA and Rec15-FLAG was also detected (Figure 14B) via co-IP experiments using a crosslinked condition, supporting the existence of an interaction between Hop1 and Rec15. I also tested whether the C-terminal-deleted Rec15-FLAG protein (Rec15ΔCT-FLAG) formed a complex with Hop1-HA by co-IP experiments, and found that Hop1-HA was no longer recovered in co-IP with Rec15ΔCT-FLAG (Figure 14B). These results suggest that the C-terminal domain of Rec15 is involved in its interaction with Hop1. Considering the previous study reported that Rec15 interacts directly with Rec10 (Miyoshi et al., 2012), Rec15-Hop1-Rec10 ternary interaction enhance the direct interaction between Rec15 and Rec10.

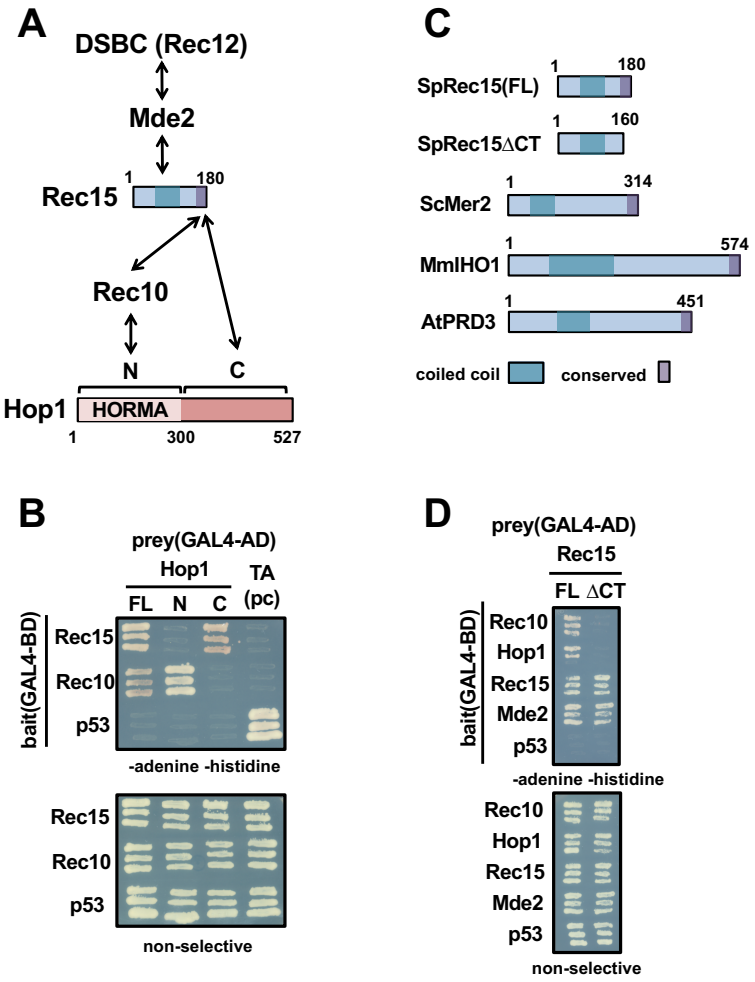

Figure 11

(A) Summary of interactions between Hop1, Rec10, Rec15, and DSBC complex. Hop1 binds to Rec10 in the N-terminus domain and to Rec15 in the C-terminus domain. Rec15 binds to both Hop1 and Rec10 in the conserved C-terminus domain. (B) Y2H assay between Hop1 and Rec10 or Rec15. Hop1 were divided into N (1-300) and C (301-527) domains (see panel A). p53 and Tantigen (Ta) were used as a positive control. (C) Structual conservation of Rec15 related proteins. Sp: *S. pombe*, Sc: *S. cerevisiae*, Mm: *Mus musculus*, At: *Arabidopsis thaliana.* Coiled coil and conserved C-terminus domains are indicated in light blue and purple boxes. (D) Y2H assay of Rec15-Full-length (FL, 1-180) and Rec15ΔCT (1-160) versus Rec10, Hop1 Rec15 and Mde2. p53 were used as a control.

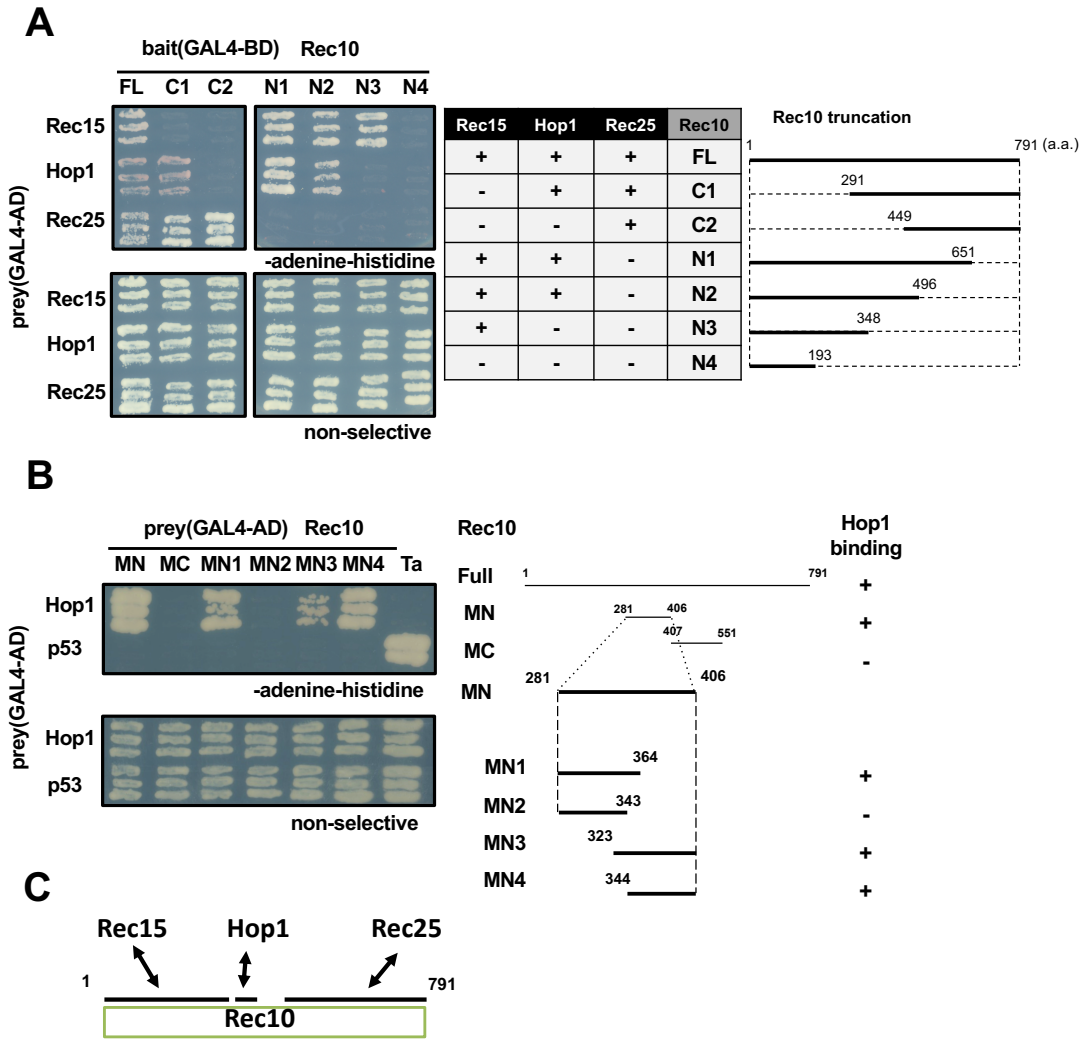

Figure 12

(A)Y2H assay between “baits” (full-length and truncated Rec10) versus *GAL4-AD* “prey” conjugated with Rec15, Hop1, or Rec25. Binding of the Rec10 fragments are summarized in the table. Positive “+”, or negative “-” (B) More detailed domain analysis of Rec10 which can interact with Hop1 by Y2H assay (C) Summary of the minimal interaction domain of Rec10 in Y2H assay.

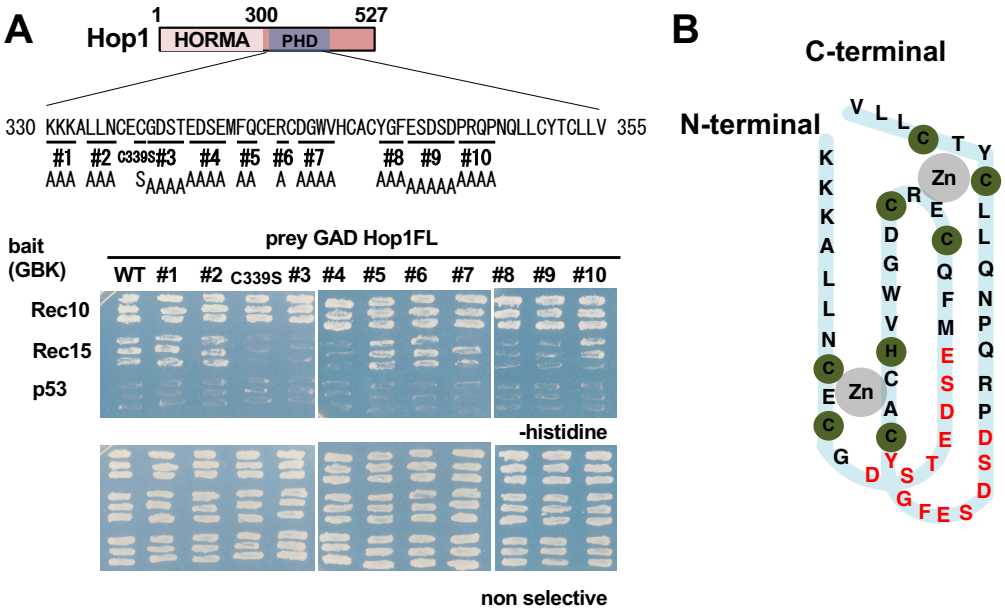

Figure 13

(A) Alanine scanning via Y2H assay to narrow down residues of Hop1 responsible for the interaction with Rec15.

(B) Putative structure of the PHD finger domain in Hop1 C-terminus domain (330-355). Red characters indicate residues of Hop1 responsible for the interaction with Rec15.

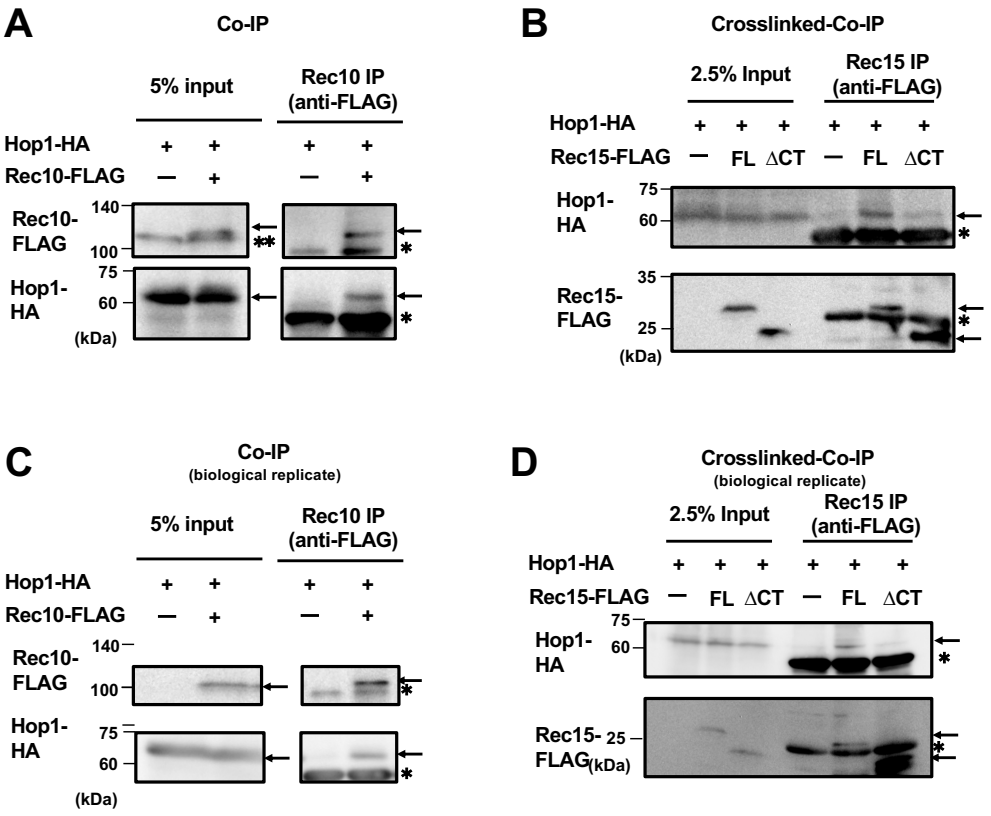

Figure 14

(A) Co-IP experiment between Rec10-FLAG and Hop1-HA. Cells were harvested at 4 hours after meiotic induction. The upper arrow indicates the position of Rec10-FLAG and the lower arrow indicates the position of Hop1-HA. Single asterisks indicate the position of immunoglobulins and a double asterisk indicates a non-specific band. The numbers in the left represent the molecular weight standards in kDa. (B) Crosslinked-Co-IP experiment between Rec15-FLAG and Hop1-HA. Cells were treated with 1% formaldehyde at 4 hours after meiotic induction. Anti-FLAG immunoprecipitation was conducted after micrococcal nuclease (MNase) treatment. The upper arrow indicates the position of Hop1-HA; the middle and lower arrows indicate the positions of Rec15-FLAG and Rec15ΔCT-FLAG, respectively. Asterisks indicates the position of immunoglobulins. (C) and (D) Biological replicates of Co-IP and Crosslinked-Co-IP experiments, respectively.

Chapter 3: Roles of Hop1 in Rec10 and Rec15 localization and DSB formation

Hop1 C-terminal domain serves as a binding interface for Rec15

To verify the possibility that Hop1 is recruited to hotspots by Rec15, I introduced alanine substitutions in the Hop1 C-terminal interface (*hop1-9A*), which destroyed its interaction with Rec15 but retained the binding interface for Rec10 (Figure 15A-C). Axis-bound Hop1-9A protein levels stayed at comparable levels to that of wild type Hop1 protein, however, Hop1-9A enrichment in DSB hotspots was considerably reduced (Figure 15D). Considering that Hop1-9A is defective in its interaction with Rec15 but is still able to interact with Rec10, Hop1 is recruited to DSB hotspots through the interaction between Hop1 and Rec15, which is reminiscent of Rec15-dependent hotspot localization of Rec10.

Rec10 localization on DSB hotspot depends on Hop1

To further understand the significance of interaction among Hop1, Rec10, and Rec15, I next investigated how Hop1, Rec15, and their interaction influence chromatin binding of Rec10. The steady state protein level of Rec10 was not affected by lack of Hop1 or Rec15 (Figure 16A). ChIP-qPCR experiments revealed that Rec10-FLAG enrichment in the axis was not significantly affected in *hop1*Δ (Figure 16B top), but interestingly, the binding of Rec10-FLAG on DSB hotspots was markedly reduced by *hop1* deletion (Figure 16B middle).

This effects of *hop1*Δ on Rec10 localization on DSB hotspots is similar to that of *rec15*Δ, which was previously reported (Miyoshi et al., 2012) (Figure 16B). Notably, in *hop1-9A* mutants, DSB hotspot-bound Rec10-FLAG was reduced, as observed in *hop1*Δ (Figure 3B). Since Hop1-9A is defective in its interaction with

Rec15 but is still able to interact with Rec10, Hop1-Rec15 interaction would assist Rec10 recruitment to the DSB hotspot.

Hop1 enhances Rec15 localization on both DSB hotspot and axis

Having shown that Rec10 requires Hop1 and Rec15 for its hotspot-localization, I next examined how Rec15 localization is affected by Hop1 and Rec10. Rec15 protein abundance in *hop1*Δ was comparable to the wild type (Figure 17A). In *hop1*Δ mutants, Rec15 localization was modestly reduced (by 30~50%) both on axis and DSB hotspot sites, and similar was the case with *hop1-9A* mutants (Figure 17B). It should be noted that *rec10*Δ confers more severe reduction of Rec15 on axis sites (Figure 17B top). These results provide the following two insights into chromatin binding of Rec15. First, DSB binding of Rec15 is partially dependent on Hop1 and Rec10. Second, axis binding of Rec15 also requires Hop1 to some extent, but more severely Rec10.

I also examined the axis and hotspot binding of the *rec15*Δ*CT* mutant. In this mutant, as shown in Figure 11D, the interactions of Rec15 with Hop1 and Rec10 were markedly reduced. ChIP-qPCR experiments revealed that Rec15ΔCT is localized to DSB hotspots at the wild type level (Figure 17B middle). However, its axis localization was markedly weakened, as previously observed in *rec10*Δ mutants (Figure 17B top) (Miyoshi et al., 2012). Therefore, Rec15 would bind to hotspots even without its C-terminal domain, but to axis sites via interactions in the C-terminal domain with Hop1 and Rec10. Taking results of Rec15 ChIP data into account, the bindings of Rec15 to both the axis and DSB hotspots are promoted by Hop1, which likely allows increased access of Rec10 to DSB hotspots (see Figure 3B and 4B).

Hop1 binding to Rec15 enhances DSB formation and recombination

Using *hop1-9A* mutants, I further investigated the contribution of Hop1-Rec15 interaction to DSB formation and the recombination frequency. As previously reported, *hop1*Δ showed partially reduced DSB formation (Latypov et al., 2010) (Figure 18). I observed that the *hop1-9A* mutant also exhibited a partial reduction of DSB formation (Figure 18). Consistent with these observations, I detected a substantial reduction of the intra-genic recombination frequency between the *ade6-M26* and *ade6-469* alleles in *hop1-9A* and *hop1*Δ (Figure 19). These results again support the notion that the interaction between Hop1 and Rec15 promotes DSB formation and meiotic.

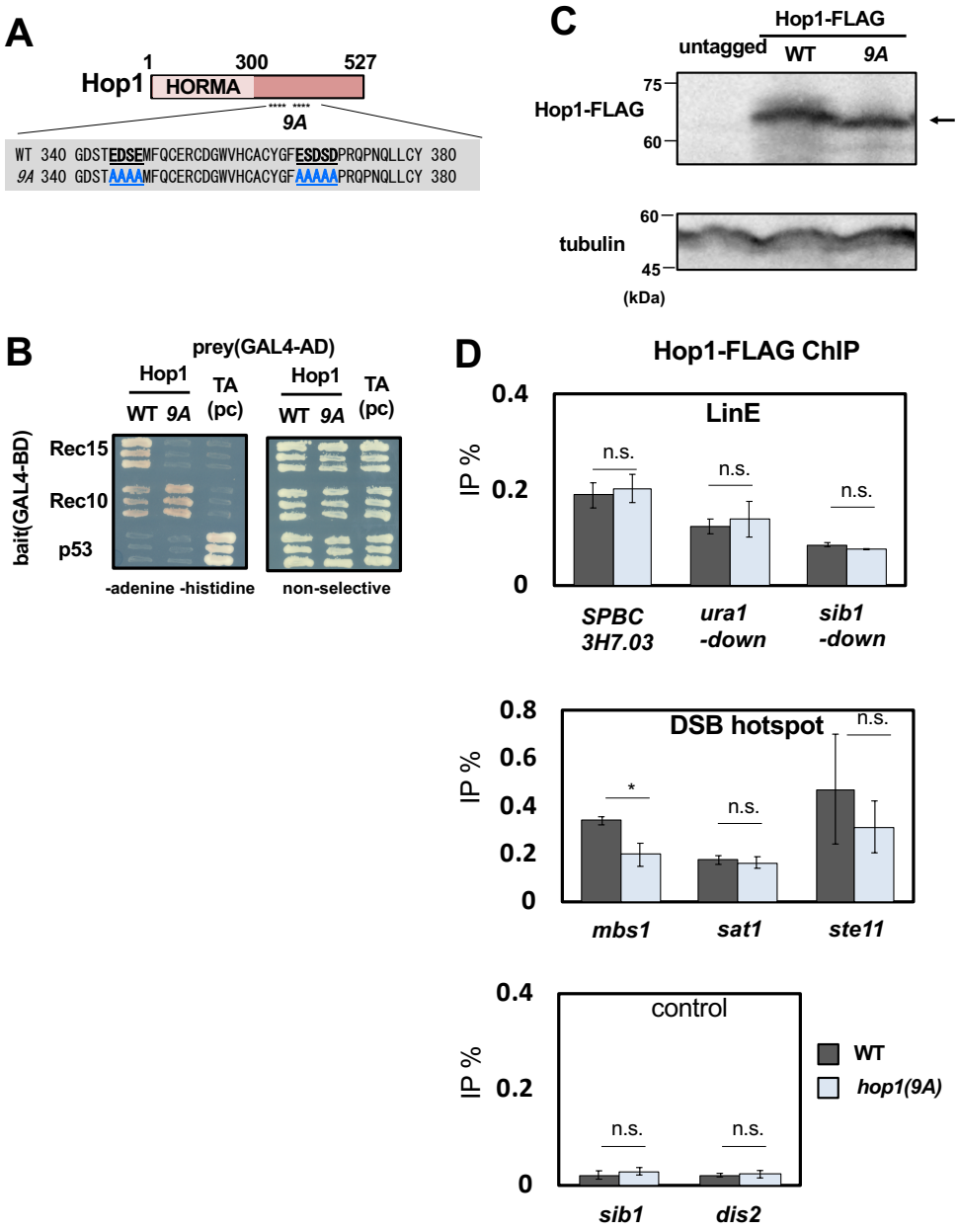

Figure 15

(A) Positions of alanine substitutions in *hop1-9A*. (B) Y2H assay of Hop1 wild type (WT) and *hop1-9A* versus Rec10 and Rec15. Upper picture: anti-FLAG blotting. Lower picture: anti-tubulin blotting. (C) Abundance of FLAG-tagged Hop1 and Hop1-9A proteins. Cells were harvested at 4 hours after meiotic induction. Proteins were detected by immunoblotting using anti-FLAG antibody. (D) Enrichment of Hop1 and Hop1-9A. ChIP-qPCR assay was performed as in Figure 9. Error bars represent the S.D. of three biological replicates. The asterisk * represents a statistical significance at <5% by two-sided Welch's t test. n.s.: not significant.

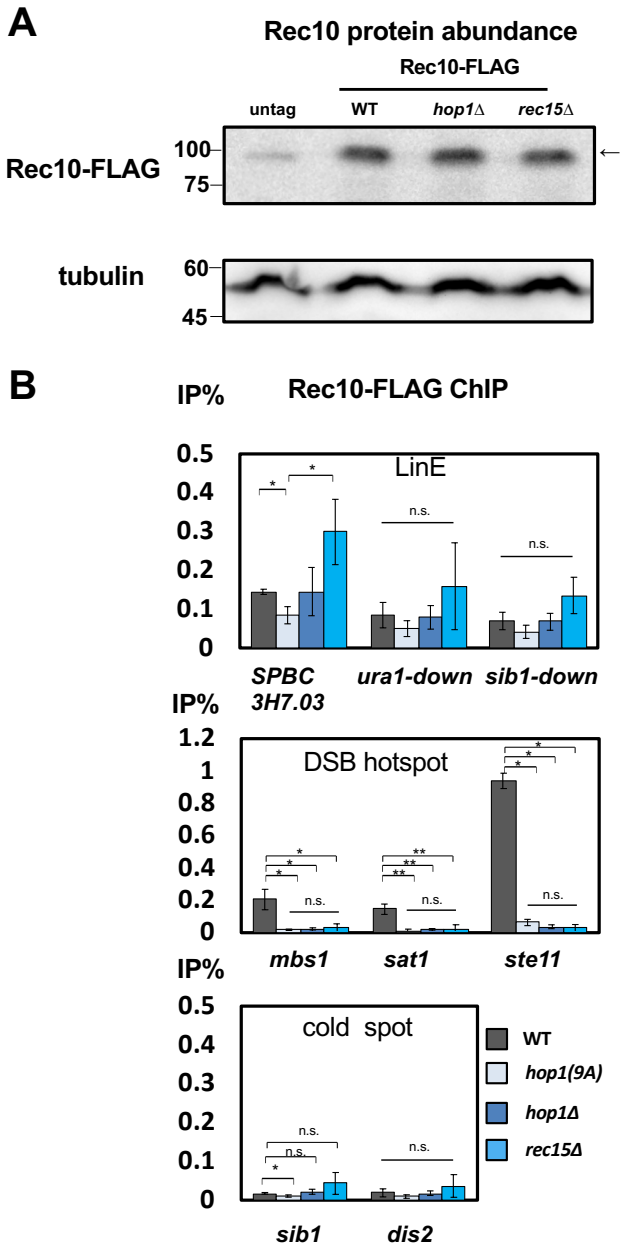

Figure 16

(A) Protein abundance of FLAG-tagged Rec10 in wild type, *hop1*Δ, and *rec15*Δ. An arrow indicates the position of Rec10-FLAG. A faint band in the control lane is a non-specific band. (B) The enrichment of Rec10-FLAG on the axis, hotspot, and control sites in wild type, *hop1*Δ, and *hop1-9A*. A ChIP-qPCR assay was performed as in Figure 10 and the primer sets for qPCR are listed and described in Table 4 and Figure 9. Error bars represent the S.D. of three biological replicates. The asterisks * and ** represent statistical significance at <5% and <1% by two-sided Welch's t test, respectively. n.s.: not significant.

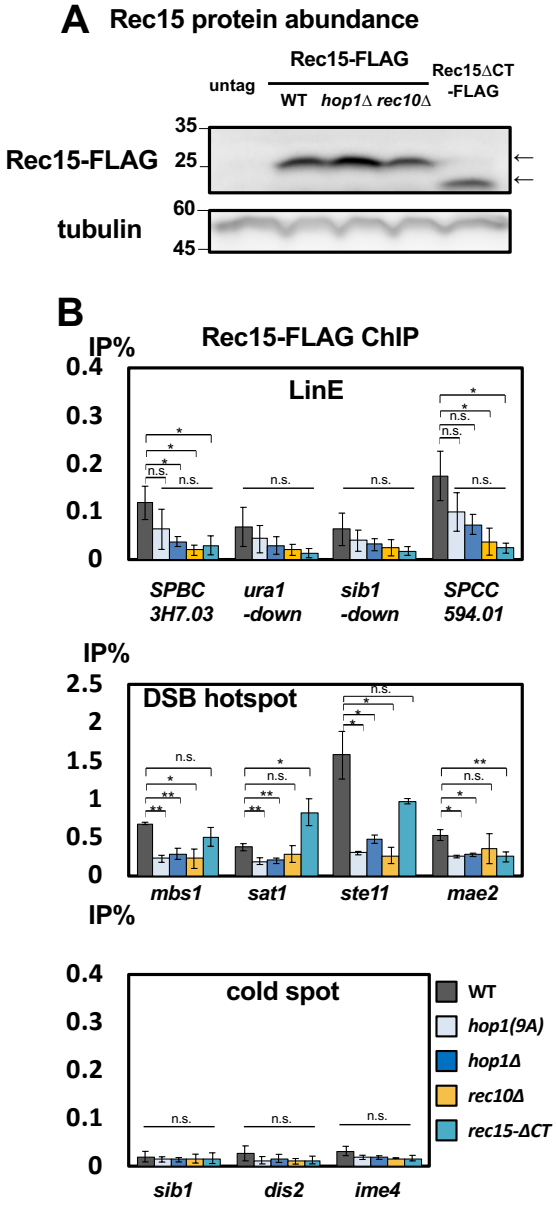

Figure 17

(A) Protein abundance of FLAG-tagged Rec15 in wild type, *hop1*Δ, and *rec10*Δ cells. Upper picture: Abundance of Rec15ΔCT-FLAG was also analysed by immunoblotting using anti-FLAG antibody. An upper arrow indicates the position of Rec15-FLAG and a lower arrow indicates the position of Rec15ΔCT-FLAG protein. Lower picture: anti-tubulin blotting. (B) Enrichment of Rec15-FLAG on axis, hotspot, and control sites in wild type, *hop1-9A, hop1*Δ*, rec10*Δ, and Rec15ΔCT-FLAG. ChIP-qPCR assay was performed as in Figure 9. Error bars represent the S.D. of three biological replicates. The asterisk * and ** denotes a statistical significance at <5% and <1% by two-sided Welch's t test, respectively. n.s.: not significant. A ChIP-qPCR assay was performed as in Figure 10 and the primer sets for qPCR are listed and described in Table 4 and Figure 9.

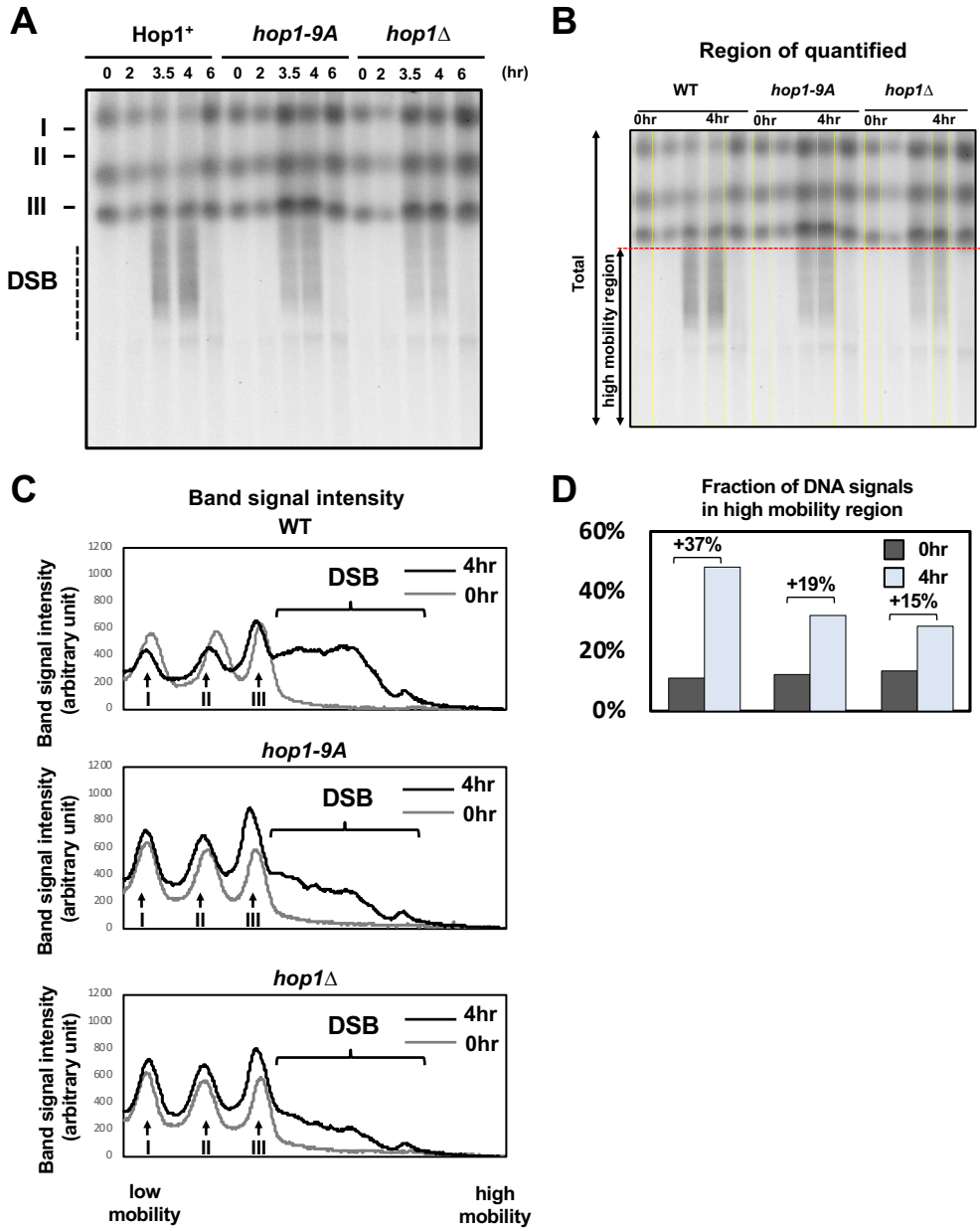

Figure 18

(A) PFGE images of wild type, *hop1-9A*, and *hop1*Δ. The numbers above the images represent the time of cell harvest (0, 2, 3.5, 4, and 6 hours after meiotic induction). The numbers in the left side of the panel indicate the position of *S. pombe* chromosomes (I, II, III). A dashed line represents DSB formation. (B) Region quantified in (C)and(D). Signals in the yellow rectangles were measured as total DNA and signals in regions under the red dotty line were measured as high mobility region in (D).(C) The intensity plots of band signals in each strains in (A) at 0hr and 4hr after meiotic induction (D) Percentage of DNA signals in high mobility region. The quantification of band signals was conducted in each strain in (A) at 0hr and 4hr after meiotic induction. Increments of the percentage are shown in top of bars.

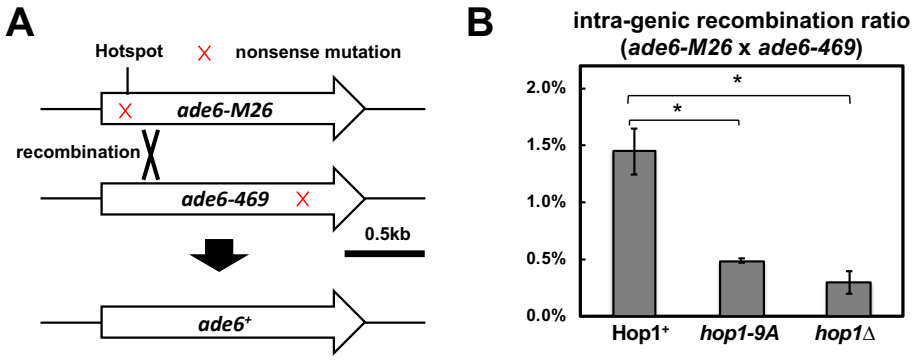

Figure 19

(A) Schematic image of the intergenic recombination between *ade6-M26* and *ade6-469* (B) Frequency of intergenic recombination frequency between *ade6-M26* and *ade6-469* measured in Hop1^{+}, *hop1-9A*, and *hop1*Δ. Error bars indicate S.D. of three biological replicates. An asterisk represents a statistical significance at <5% by Bonferroni-corrected multiple t-test, respectively.

Chapter 4: Hop1 provide redundant pathway between axis and Spo11 complex

Impact of *hop1*Δ on localization of Rec10 and Rec15 is milder compared to *rec10*Δ and *rec15*Δ

So far, I have demonstrated that Hop1 enhances DSB formation via its interaction with Rec10 and Rec15, affecting localization of both Rec10 and Rec15. However, ChIP-qPCR experiment in this study revealed that *hop1*Δ showed a less marked reduction in Rec10-FLAG enrichment in DSB hotspots than *rec15*Δ (Figure 20A). Genome wide analysis of Rec10 localization in *hop1*Δ and *rec15*Δ showed Rec10 on DSB hotspots slightly remain in *hop1*Δ, compared to *rec15*Δ, supporting this notion (Figure 20B and C). Similarly, localization of Rec15 was partially reduced in *hop1*Δ, while *rec10*Δ caused severe reduction of Rec15 on axis (Figure 21A). I also confirmed Rec15 localization partially reduced in *hop1*Δ both at axis sites ant DSB hotspot sites, while axial localization of Rec15 was almost diminished in *rec10*Δ (Figure 21B and C).

Analysis so far indicates impact of *hop1*Δ was milder than those of *rec10*Δ and *rec15*Δ. This is consistent with previous studies reporting that DSBs are absent in *rec10*Δ and *rec15*Δ, but not in *hop1*Δ (Ellermeier and Smith, 2005; Latypov et al., 2010; Lin and Smith, 1995). Previous study showed Rec10 and Rec15 mutually affect their localization via their direct interaction (Miyoshi et al., 2012) (see Figure11 and Figure 12). Then, how Rec10-Hop1-Rec15 interaction and Rec10-Rec15 direct interaction contribute to the interaction between Spo11 complex and axial components?

Hop1 and Rec10 redundantly recruit Rec15 onto axis

In order to assess the contribution of Rec10-Rec15 interaction and Rec10-Hop1-Rec15 interaction, I generated "separation-of-function" mutants of Rec10, which lost its interaction to specifically Rec15 or Hop1, because my data have shown that Rec10 is required for Hop1 localization on axis and DSB hotspot, deletion of Rec10 disrupts both Rec10-Rec15 interaction and Hop1 function.

According to the detailed Y2H-based domain analysis, Rec10 interacts with Rec15 by its N-terminus domain and binds with Hop1 in its middle region (see Figure 11). In order to get insight of N-terminus region of Rec10, I submitted N-terminus of Rec10 (201-400) amino acid sequence to PHYRE2 server (http://www.sbg.bio.ic.ac.uk/phyre2/) (Kelley et al., 2015). Then the structure of erythroid membrane protein 4.1r (PDB ID 1GG3) was obtained as the model of Rec10 N-terminus structure. The predicted structure of Rec10 N-terminus is quite similar to the structure of mammalian Rec10 homolog SYCP2, whose structure has been recently solved (Feng et al., 2017) (Figure 22A). Although structure of SYCP2 is available, there is not enough information of binding surface of SYCP2. Therefore, I employed the C-lobe of erythroid membrane protein 4.1r, whose binding surface has been well characterized (Han et al., 2000). As erythroid membrane protein 4.1r binds to its binding partner p55 via its binding pocket including Glutamate 246, Glutamate 309 residue of Rec10 corresponding to Glutamate 246 in erythroid membrane protein 4.1r were mutagenized.

For Rec10 mutant of Hop1 binding, I mutated residues based on the previous study of budding yeast Hop1 and conservation of HORMAD binding peptide (Figure 22B). In budding yeast, Rec10 homolog Red1 K348 is essential for its binding to Hop1 (Woltering et al., 2000). In order to apply this information to fission yeast Rec10, we aligned Rec10 and Red1 based on the previous study (West et al., 2018). As the homology between

fission yeast Rec10 and budding yeast Red1 is weak, we also referred to Mad2 binding consensus "R/KψψXφxxP"(Rosenberg and Corbett, 2015). Among Rec10 residues, we chose P348 from the comparison to Mad2 binding consensus and K349 from the homology to budding yeast Red1 K348.within the middle region of Rec10 ($\underline{K}_{339}\underline{L}_{340}\underline{L}_{341}P_{342}A_{343}\underline{I}_{344}I_{345}V_{346}S_{347}\underline{P}_{348}K_{349}$). Then I mutated 2 residues P348 and K349 to alanine (*rec10-P348GK349G*).

Y2H assay showed the newly isolated point mutants of Rec10 lost interaction with Rec15 (*rec10-E309A*) and Hop1 (*rec10-P348GK349G*) (Figure 22C). Both mutant proteins exhibited nuclear localization comparable to wild type proteins, which is indicative of their localization in the axis (Figure 23A), and the amount of protein was comparable to the wild type Rec10 (Figure 23B).

Although interaction of Rec10-309A and Rec15 were not observed by Y2H assay, Hop1 expressed in Y3H assay bridged between Rec10-309A and Rec15 (Figure 24). Accordingly, the *rec10-E309A* and *rec10-P348GK349G* mutants exhibited a moderate reduction of intra-genic recombination frequency between the *ade6-M26* and *ade6-469* alleles recombination frequency compared to *hop1*△ (Figure 25). When the meiotic recombination frequency in a double mutant for *hop1*△*, rec10-P348GK349G* was examined, I observed very similar levels of reduction in recombination frequency as in the *hop1*△ single mutant.

More importantly, the *hop1*△ and *rec10-E309A* double mutant showed undetectable levels of recombination frequency and very low spore viability (Figure 25). Pulsed field gel electrophoresis analysis revealed a marked reduction of DSB frequency in the *hop1*△ and *rec10-E309A* double mutant (Figure 26), as seen in the *rec10*△ mutant. These data suggest two redundant pathways for spo11 complex interaction to axis:

one via direct binding between Rec10 and Rec15, and the other through the assistance of Rec10-Hop1-Rec15 interactions.

Consistent with this idea, Rec15ΔCT, which lost interaction to both Hop1 and Rec10, also showed undetectable levels of recombination frequency and very low spore viability (Figure 25).

Prediction of conservation of Rec10-Hop1-Rec15 ternary complex in other organisms

It would be intriguing to know if Rec10-Hop1-Rec15 ternary complex is conserved among species. In fission yeast and mouse, some of interaction are conserved (De Los Santos and Hollingsworth, 1999; Stanzione et al., 2016). In order to obtain any clue for hidden interaction, I conducted the secondary structure prediction of Rec10 (fission yeast), Red1 (budding yeast), and SYCP2 (mouse). Then I found that N-terminal of those proteins resemble each other in their secondary structures (Figure 27). Notably, the position of Rec10 mutations, which destroys interaction with Rec15 or Hop1, is located within this conserved structure. It is indicative of conservation of ternary complex among species (Figure 28).

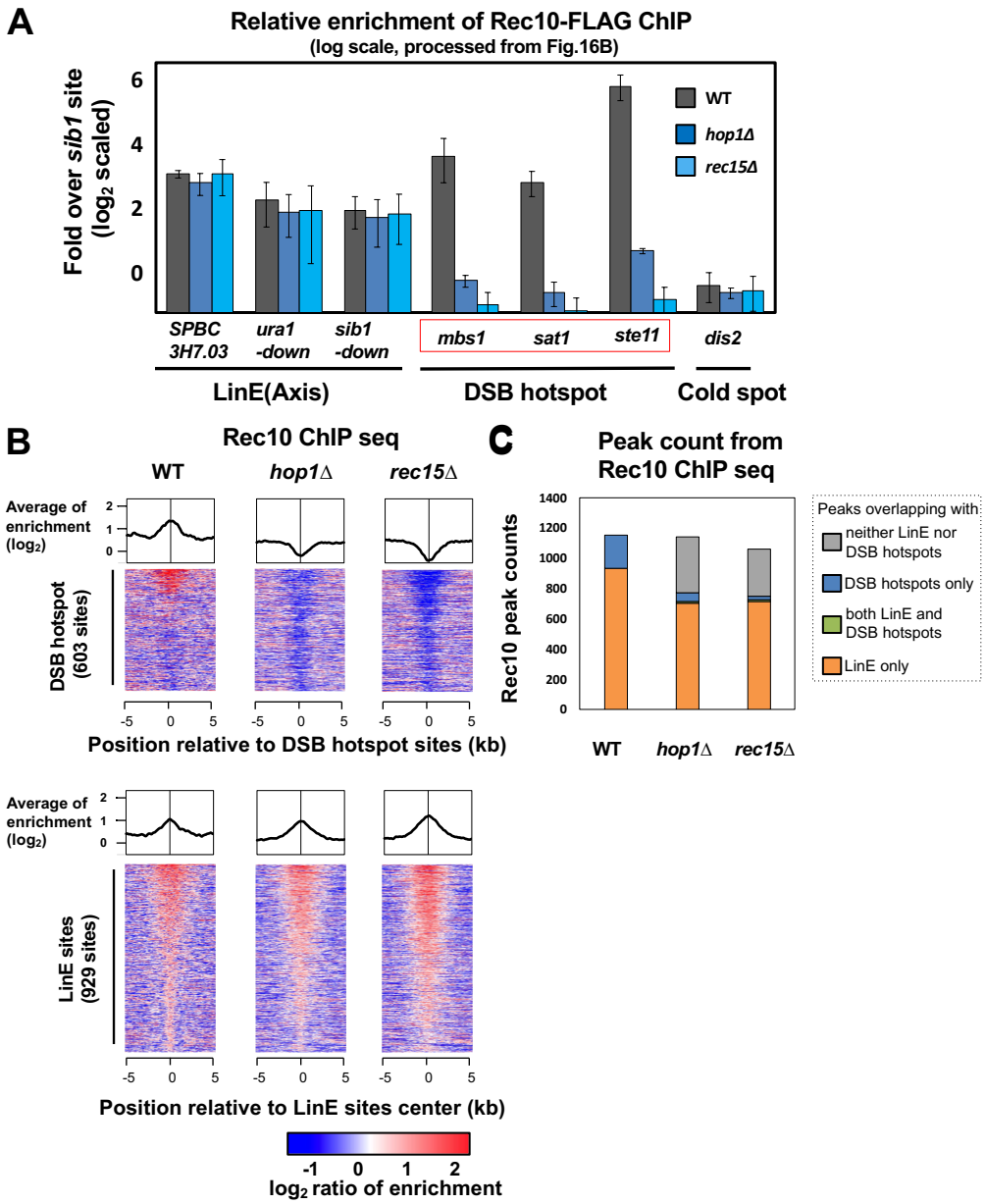

Figure 20

(A) Normalized fold enrichment of Rec10-FLAG on axis, hotspot, and control sites in wild type, *hop1*Δ, *rec15*Δ. Raw ChIP-qPCR data is form Figure 16. The IP/WCE values of cold spot site *sib1* were used as the background signal for normalization. (B) Heat map images of ChIP-seq signals of Rec10 around DSB hotspot sites and LinE sites in wild type, *hop1*Δ, and *rec15*Δ. DSB hotspots are sorted by Rec12-oligo counts reported in the previous study (Fowler et al., 2013). LinE sites are sorted by Rec10 ChIP fold enrichments. ChIP-seq experiments were conducted as in Figure 3 and 7B. (C) Stacked bar graph of numbers of Rec10 peaks in wild type, *hop1*Δ, and *rec15*Δ. Called peaks were classified according to their overlaps with LinE sites or DSB hotspots.

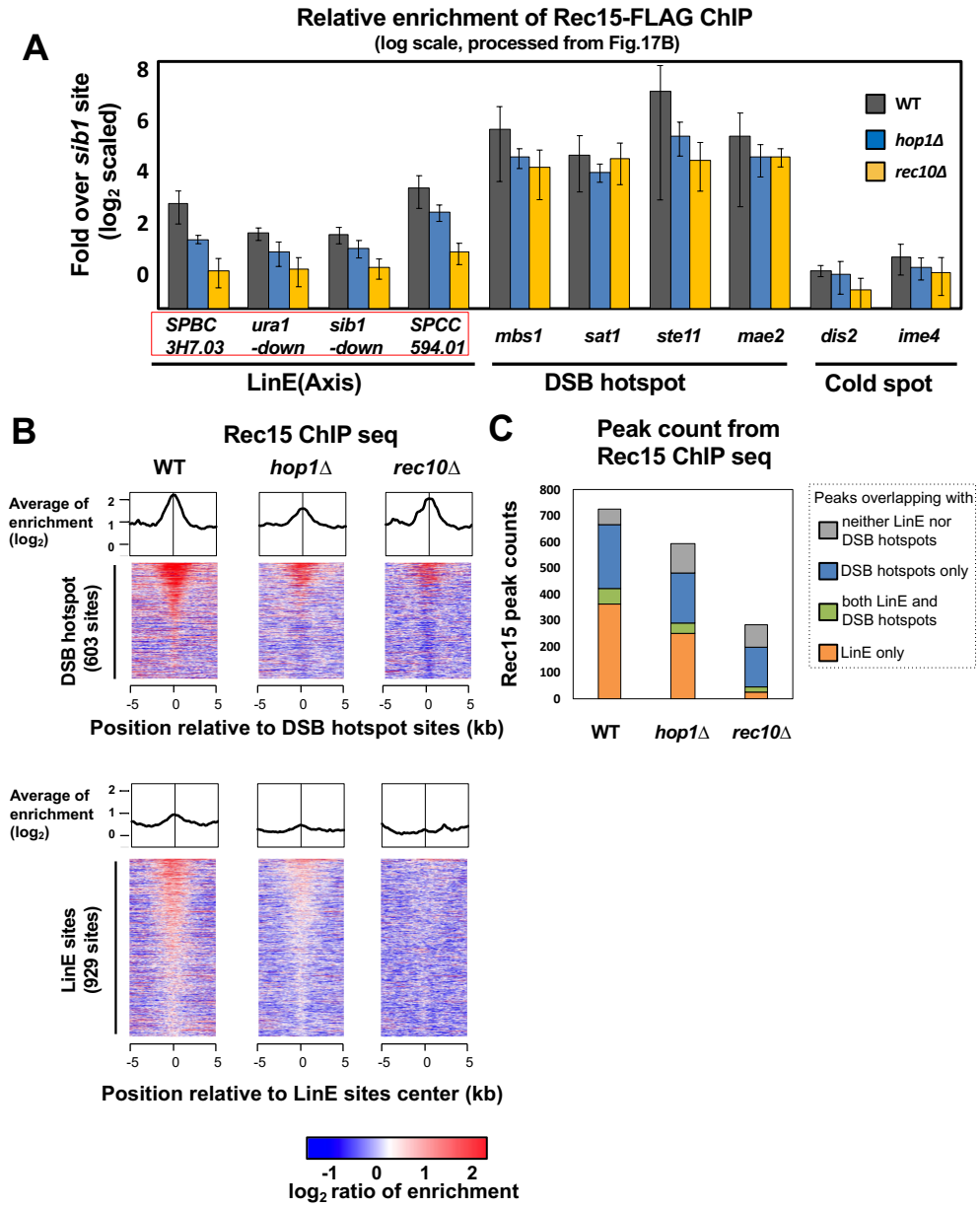

Figure 21

(A) Normalized fold enrichment of Rec15-FLAG on axis, hotspot, and control sites in wild type, *hop1*Δ, *rec10*Δ. Raw ChIP-qPCR data is form Figure 17. The IP/WCE values of cold spot site *sib1* were used as the background signal for normalization. (B) Heat map images of ChIP-seq signals of Rec15 around DSB hotspot sites and LinE sites in wild type, *hop1*Δ, and *rec10*Δ. Drawing of heat maps are as in Figure 20B. ChIP-seq experiments were conducted as in Figure 3 and 7B. (C) Stacked bar graphs of numbers of Rec15 peaks in wild type, *hop1*Δ, and *rec10*Δ. Called peaks were classified according to their overlaps with LinE sites or DSB hotspots.

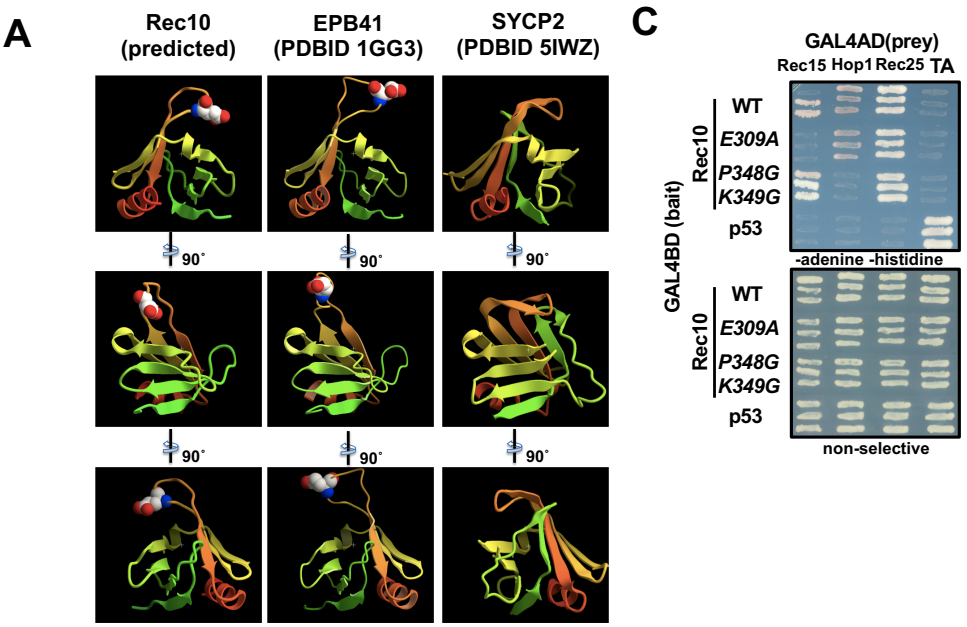

B

Mad2 binding		**R**	
Consensus		**Kψψ φ P**	
HsMad1		TKVL-HMSLNPT	
ScMad1		IRIL-QLRDGPF	
SpMad1		CRVL-QHRSNPT	
DmMad1		FKVV-HFSENPA	
HsCdc20		AKIL-RLSGKPQ	
ScCdc20		KRIL-QYMPEPK	
SpSlp1		TRVLAFKLDAPE	
DmFzy		LKVV-YSIKTPI	
SpRec10	337	NKLLPAIIVSPK	349

ψ ... aliphatic residues (IVLM)
φ ... hydrophobic residues (IVLMF)

Figure 22

(A) The structure of EPB4.1, which is the model of Rec10 structure prediction (left). Emphasized residue is glutaminase 246, which is binding surface of p55, the interactor of EBP4.1. Middle is the predicted structure of Rec10 N-terminal region. Emphasized residue is glutaminase 309, which was introduced mutation. Right is structure of SYCP2 N-terminal region in previous study (Feng et al.,2017). Prediction of Rec10 N-terminal structure is consistent with the structure of SYCP2. (B) Alignment of HORMA-domain binding sequence of Mad1, Cdc20 (Slp1 homolog of fission yeast) and fission yeast Hop1. Yellow highlight is Mad2 binding consensus motif (R/KψψxφxxxP), where ψ indicates aliphatic residue, φ indicates hydrophobic residues, and x indicates any residues. Red letters indicate Hop1 sequence mutated residues. (C) Y2H assay between Rec10 mutants versus Rec15, Hop1, and Rec25.

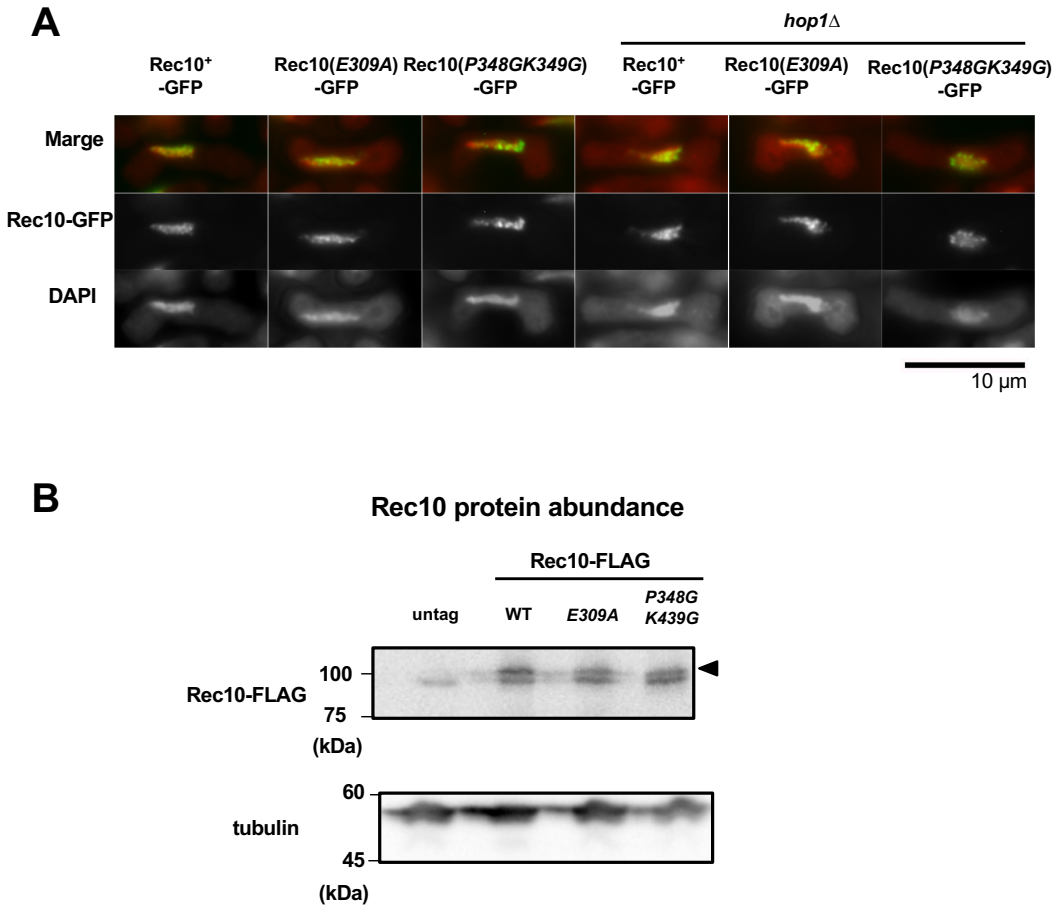

Figure 23

(A)Microscopic observation of GFP-tagged Rec10. Cells were cultured in a sporulation medium, fixed, stained by DAPI, and observed during meiotic prophase. The Scale bar indicates 10μm. (B) Protein abundance of Rec10-FLAG, Rec10-E309A, and Rec10-P348G K439G. An arrowhead indicates the position of the Rec10-FLAG band.

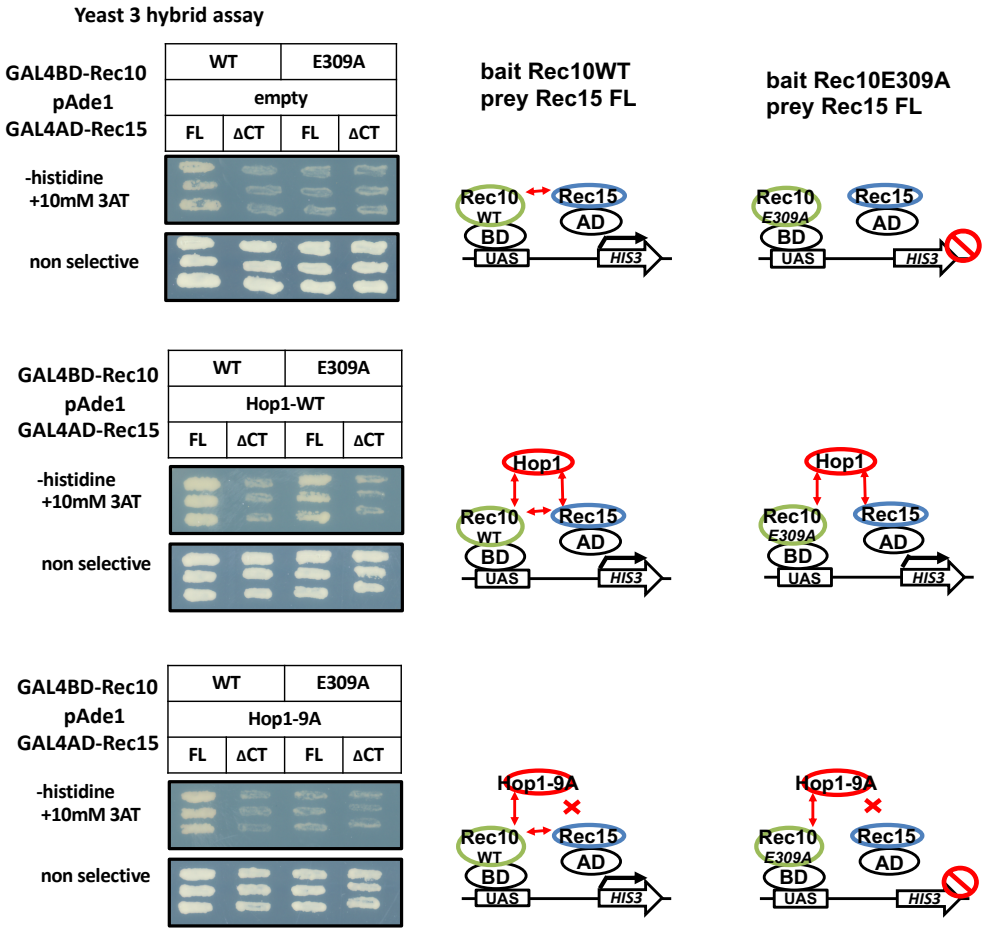

Figure 24

Yeast 3 hybrid experiments indicating tripartite interaction among Rec10, Rec15 and Hop1.

(top) Rec10 and Rec15 interacts directly and Rec10E309A mutant lost ability to bind Rec15.

(middle) Expression of Hop1 restored interaction between Rec15 and Rec10 E309A, which indicates that Hop1 mediates interaction between Rec10 and Rec15.

(bottom) Expression of Hop1-9A which is deficient in Rec15 binding did not restore interaction between Rec15 and Rec10 E309A, which indicates that mediator function of Hop1 depends on its ability to bind to Rec15.

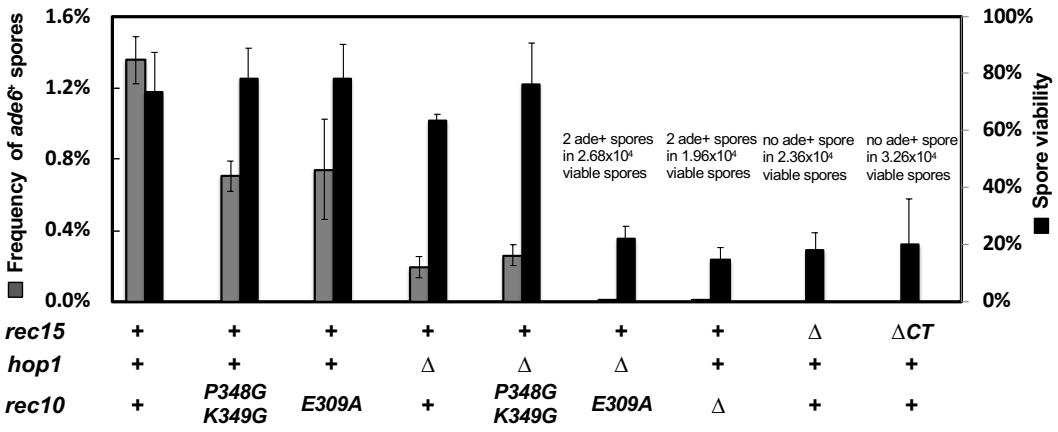

Figure 25

Synthetic recombination and sporulation defect in *rec10E309A* and *hop1*Δ. Intergenic recombination frequency between *ade6-M26* and *ade6-469* (gray bars, scale indicated in left Y-axis) and spore viability (black green bars, scale indicated in right Y-axis) were measured. Error bars represent S.D. of several biological replicates (5 in wild type, 3 in *rec10P348GK349G*, *rec10E309A, hop1*Δ, and *hop1*Δ *rec10P348GK349G*, 4 in *hop1*Δ *rec10E309A, rec10*Δ and *rec15*Δ, and 3 in *rec15*Δ*CT*.

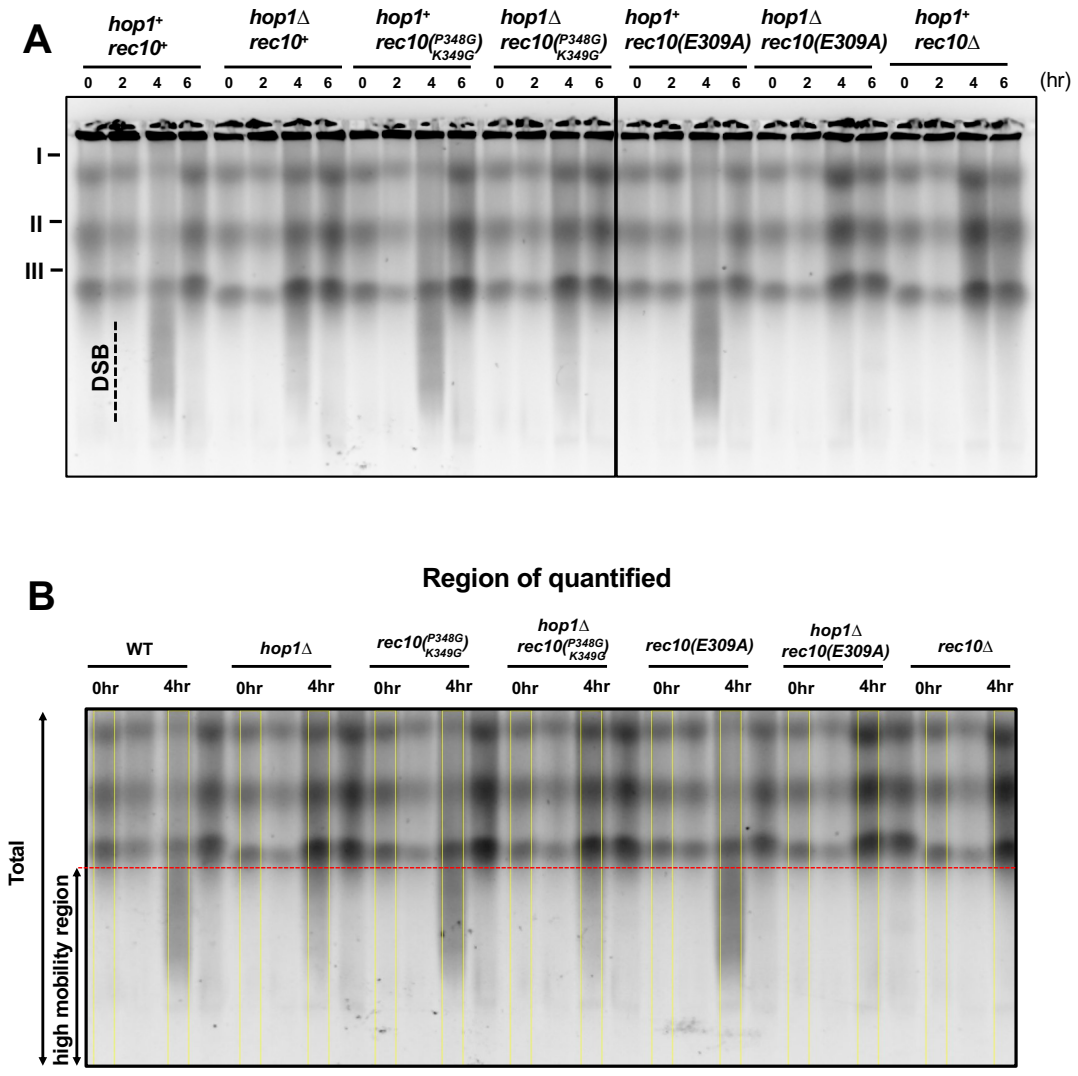

(continues to next page)

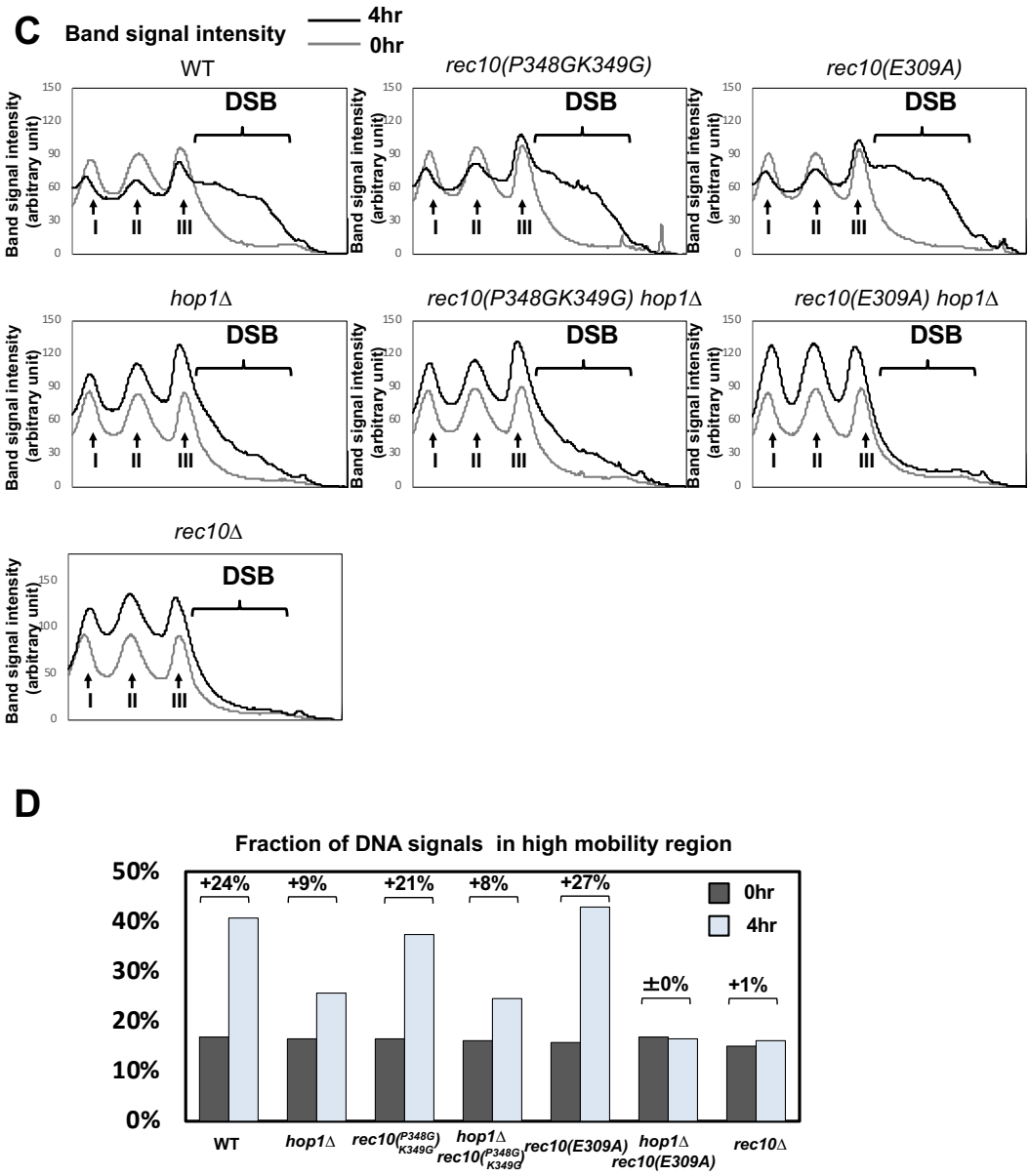

Figure 26

. (A) PFGE images for the detection of meiotic DSBs in wild type, *hop1*Δ, *rec10P348GK349G*, *hop1*Δ*-rec10 P348GK349G* double mutant, *rec10E309A*, *hop1*Δ*-rec10E309A* double mutant, and *rec10*Δ. The numbers above the images represent the time of cell harvest (0, 2, 4 and 6 hours after meiotic induction). The numbers in the left side of the panel indicate the position of *S. pombe* chromosomes (I, II, III). A dashed line represents DSB formation. (B) Region quantified in (C) and (D). Signals in the yellow rectangles were measured as total DNA and signals in regions under the red dotty line were measured as high mobility region in (D).(C) The intensity plots of band signals in each strains in (A) at 0hr and 4hr after meiotic induction (D) Percentage of DNA signals in high mobility region. The quantification of band signals was conducted in each strain in (A) at 0hr and 4hr after meiotic induction. Increments of the percentage are shown in top of bars

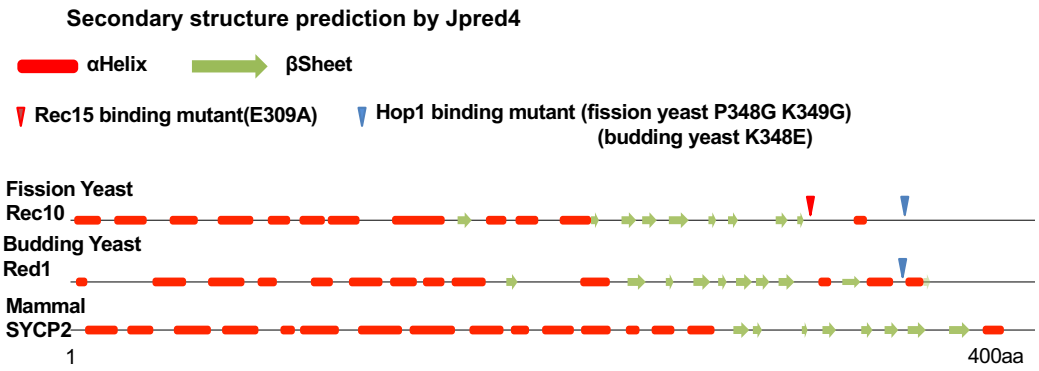

Figure 27

The secondary structure prediction of the N terminus (1-400 amino acids) of fission yeast Rec10, budding yeast Red1, and mammalian SYCP2 were analysed by J pred4. Red and green rectangles represent positions of α-helix and β-sheet, respectively. Red and blue arrowheads indicate positions of E309A and P348G K349G, respectively.

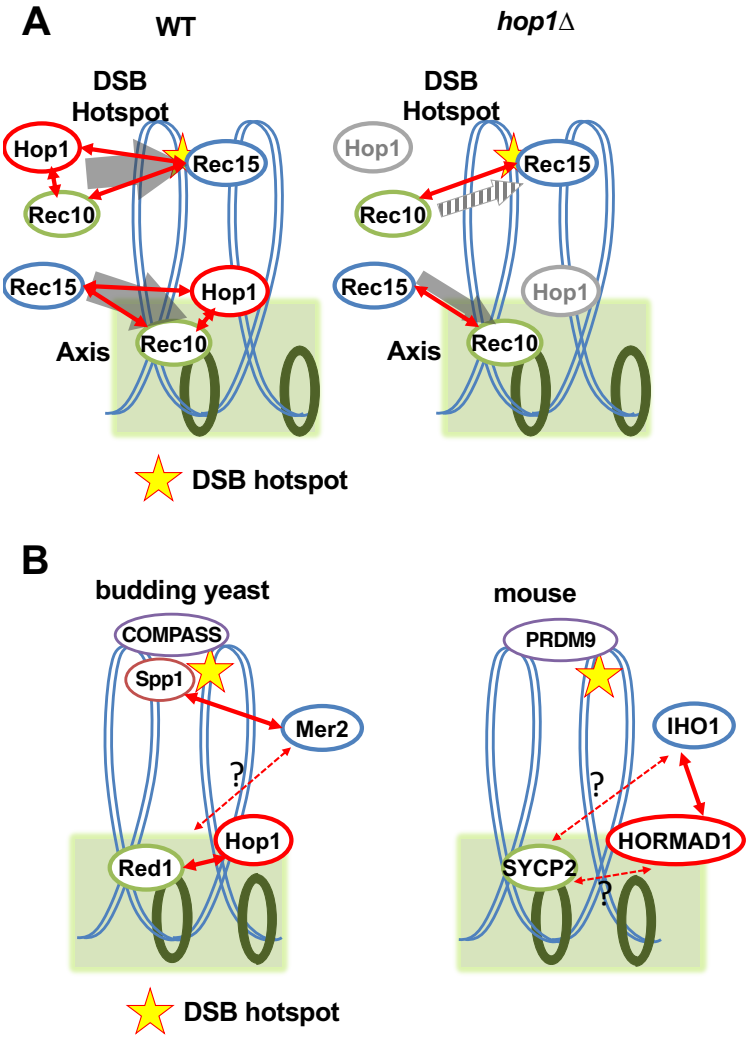

Figure 28

(A) Schematic diagram of redundant pathways of Rec15 recruitment by Rec10 in the presence (right) or absence (left) of Hop1. Red arrow indicates protein interaction and grey arrow indicates the amount of recruitment. (B) Known interactions among homologues of Rec15, Rec10 and Hop1 in budding yeast and mouse.

4. Discussion

The role of Hop1 in the maturation of meiotic chromosome

The data in this study suggest that the fission yeast axis protein Hop1 promotes interaction of the axial protein Rec10 (corresponding to Red1 in budding yeast) to DSB hotspots, and Rec15 (a member of the DSB-forming complex) localization on chromatin via its interaction with both Rec10 and Rec15. The previous study reported direct interaction between Rec10 and Rec15 recruits Rec10 to DSB hotspot and Rec15 to axis (Miyoshi et al., 2012). These results, along with previous studies, the interaction between Hop1 and Rec15 serves as the secondary pathway for establishing DSB-competent meiotic chromosomes.

In addition, results in this study suggest that after DNA replication the axis is sequentially established by cohesin Rec8 and then Rec10, followed by the participation of Hop1. This idea is supported by the following three observations: 1) the axial localization of Rec10 is severely affected by the deletion of Rec8 (Lorenz 2004;Miyoshi et al, 2012); 2) in the Rec10 deletion, the axis localization of Hop1 disappears (see Figure 9B) and has a strong effect on DSB formation and recombination frequency; 3) in the *hop1* deletion strain, the axial localization of Rec10 is only slightly affected (Figure 15B); 4) Rec15 is required for axis binding of neither Rec10 (Figure 16B) nor Hop1 (Figure 10B). Such a hierarchy is consistent with the previous observations of budding yeast (Sun et al., 2015; Panizza et al., 2011). The sequential action of Rec10 to Hop1 suggests that the *rec10* deletion confers a stronger phenotype for recombination and DSB formation than mutations of the same axial factor Hop1 (Ellermeier et al. 2005; Latypov et al. 2010).

Hop1 mediated interaction between Spo11 complex and axis component

I have experimentally demonstrated that the interaction between Rec15 and Rec10, a member of Spo11 complex and the main component of the axis, respectively, is supported by dual pathway; one via the direct interaction between Rec10 and Rec15, another via Hop1 mediated Rec10-Hop1-Rec15 ternary interaction. This notion is supported by the analyses using separation-of-function mutations of Rec10 for its interaction with either Rec15 or Hop1 (see Figures 25 and 26). In the *rec10-E309A* mutation lacking Rec10-Rec15 interaction, meiotic recombination frequency decreased to about 50% of the wild type, while the overall DSB level was only limitedly affected. In the *rec10-P348G K349G* mutant, which results in a deficient Rec10-Hop1 interaction, meiotic recombination frequency also decreased to 50% of the wild type. The combination of *hop1*△ and *rec10-E309A* led to the complete abolishment of meiotic recombination and DSB formation. Therefore, it is very likely that the interactions of Rec10-Rec15 and Hop1-Rec15 play redundant roles in DSB formation. This notion is consistent with Y3H data showing that the interaction between Rec10-E309A and Rec15 was recovered when Hop1 was additionally expressed (see Figure 24).

However, this does not suggest that Hop1 plays only a supplementary role. It should be noted that Hop1 interacts with both Rec10 and Rec15. I propose that Hop1 not only acts as a backup molecule, but probably also plays a role as a molecular matchmaker to promote the interaction between Rec15 and Rec10. Indeed, when I introduce the *hop1-9A* mutation, which diminishes the interaction between Hop1 and Rec15 only but not between Hop1 and Rec10 (see Figure 15), I observed substantial defects in DSB formation, recombination frequency, and binding of Rec15 to axis, as observed in the *hop1*△ mutant, though the axis localization of Hop1-

9A protein itself was influenced very little. The role of Hop1 as a molecular matchmaker may not be essential, but it certainly plays an important regulatory function to activate DSB hotspots.

TLAC model and Hop1

In the previous study, it has been reported that Rec10 and Rec15 localize on both axis sites and DSB hotspot sites, and this observation was interpreted as tethered loop axis complex (TLAC see Figure 2). Here I demonstrated that in absence of Hop1, Rec10 localization on DSB hotspot is diminished and Rec15 localization on both DSB hotspot and axis sites are reduced. Together with the previous study, it is plausible that Hop1 facilitates the formation of TLAC via its interaction with Rec15 and Rec10. As budding yeast axial protein Red1, Hop1 and fission yeast Hop1 are involved in the process after DSB formation, such as crossover and non-crossover choice (Brown et al., 2018; Medhi et al., 2016), it is plausible that the contact of axis proteins to the DSB hotspot site is beneficial for the coupling of DSB formation and the subsequent recombination processes at the same location.

Role sharing of Hop1 and Rec10 in Spo11 complex recruitment

The HORMA domain of Hop1 is also found in the spindle assembly checkpoint protein Mad2 in centromeres and is known to enable the dynamic dissociation of centromeres depending on spindle checkpoint (Vader and Musacchio, 2014). Rec10, along with Rec25, and Rec27 proteins build the axis structure near the binding sites of cohesin Rec8 (Davis et al., 2008; Fowler et al., 2013; Phadnis et al., 2015; Sakuno and Watanabe, 2015).

Therefore, it is plausible that binding kinetics of Hop1 protein is dynamic, while that of Rec10 is static. Hop1 may have a dynamic and regulatory function and be responsible for controlling the amount of DSB depending on the cell cycle, checkpoint, and chromosome domains, compared to the more static function of Rec10.

Evolutionary conservation of axial components, DSB forming complex, and their interactions

The results of this study suggest the presence of a universal mechanism for the interaction between Spo11 complex and axis components in eukaryotes to activate meiotic DSB formation. Recent studies have revealed that most of the factors related to meiotic DSB formation are evolutionarily conserved (see Table 1). For instance, Rec15 and Hop1 have orthologues such as budding yeast Mer2/mammalian IHO1 and budding yeast Hop1/mammalian HORMAD protein, respectively. In particular, mammalian IHO1 has been identified as a specific binder of HORMAD1 (Stanzione et al., 2016), though the interaction between *S. cerevisiae* Hop1 and Mer2 has yet to be demonstrated. The homologue of Rec10 in budding yeast is Red1. It is assumed that the mammalian Rec10/Red1 counterpart may be a synaptonemal and axial protein, SYCP2 (see Figure 27). The N-terminal domains of these Rec10 homologues are predicted to form a common secondary structure. In budding yeast, the interaction between Red1 and Hop1 has been reported (De Los Santos and Hollingsworth, 1999; West et al., 2019), and an analysis on mouse previously demonstrated that HORMAD1 protein interacts with SYCP2/3 (Fukuda et al., 2010), consistent with the results that fission yeast Hop1 interacts with Rec10.

It is likely that the domains involved in these intermolecular interactions are at least structurally conserved. For example, the C-terminal domain of Rec15, which is responsible for the interaction with Hop1, is conserved

in various taxa including fungi, mammals, and plants (Tessé et al., 2017). The interface of Rec10 for Rec15 binding is also preserved in fungi and mammals in terms of predicted secondary structure (see Figure 27). The domain of Rec10 for its interaction with Hop1 is also located at close proximity to the conserved C-terminal domain. The proximity of the two interaction domains of Rec10 for Rec15 and Hop1 suggests synergistic mechanisms for DSB regulation by Rec15 and Hop1.

Since fission yeast does not form the authentic SC structure, the functions of *S. pombe* Hop1 are likely to be simplified to their roles in DSB formation. However, such conserved domains of Hop1/HORMAD1 proteins in budding yeast and mammals have more diverse roles in meiotic recombination, such as in SC formation and DSB homeostasis. The Hop1/HORMAD1 may be presumably coupling DSB formation with the cell cycle, meiotic DSB checkpoint, and chromosomal domain structure though its regulatory mechanism yet to be known. It would be intriguing future experiments to introduce point mutations in the conserved domains of mammalian and budding yeast Hop1 to evaluate the influence on meiotic DSB formation and recombination.

5. Conclusion

Meiotic recombination is one of the most crucial steps during meiosis. Meiotic recombination is initiated by double strand breaks (DSBs) on DNA. DSB is introduced by conserved type II topoisomerase-like complex Spo11. Spo11 and its activity are well controlled by the chromosome axis.

Hop1 is a meiotic axial protein, which contains conserved HORMA domain and governs multiple processes of meiosis. Among various functions of Hop1, the promotion of DSB formation is one of the fundamental roles.

In this thesis, I analysed roles of Hop1 on meiotic DSB formation in fission yeast *Schizosaccharomyces pombe*, in which the role of Hop1 is limited to DSB formation only. Then I made four discoveries. First, Hop1 localizes on both the chromosomal axis and DSB hotspot. Second, Hop1 interacts with spo11 complex protein Rec15 and axis protein Rec10. Third, Hop1 serves as the matchmaker of Rec15 and Rec10, promotes interaction between axis and spo11 complex and thus enhances DSB formation. Last, Rec15 interacts both axial protein Hop1 and Rec10, providing two ways of recruitment of Spo11 complex onto the axis.

Here I revealed Hop1, Rec10, and Rec15 interact with each other and the interaction promotes DSB formation in *S. pombe*. As all of three proteins are conserved among species, the interaction between three proteins can be conserved in other organisms. In contrast to *S. pombe*, Hop1 in other organisms have multiple roles other than DSB formation. Therefore, more complicated mechanisms might exist in other organisms.

6. References

Acquaviva, L., Székvölgyi, L., Dichtl, B., Dichtl, B.S., Saint André, C.D.L.R., Nicolas, A., and Géli, V. (2013). The COMPASS subunit Spp1 links histone methylation to initiation of meiotic recombination. Science.339, 215–218.

Arora, C., Kee, K., Maleki, S., and Keeney, S. (2004). Antiviral protein Ski8 is a direct partner of Spo11 in meiotic DNA break formation, independent of its cytoplasmic role in RNA metabolism. Mol. Cell 13, 549–559.

Baudat, F., Buard, J., Grey, C., Fledel-Alon, A., Ober, C., Przeworski, M., Coop, G., and De Massy, B. (2010). PRDM9 is a major determinant of meiotic recombination hotspots in humans and mice. Science. 327, 836–840.

Bergerat, A., De Massy, B., Gadelle, D., Varoutas, P.C., Nicolas, A., and Forterre, P. (1997). An atypical topoisomerase II from archaea with implications for meiotic recombination. Nature 386, 414–417.

Bhatt, A.M., Lister, C., Page, T., Fransz, P., Findlay, K., Jones, G.H., Dickinson, H.G., and Dean, C. (1999). The DIF1 gene of *Arabidopsis* is required for meiotic chromosome segregation and belongs to the REC8/RAD21 cohesin gene family. Plant J. 19, 463–472.

Blat, Y., Protacio, R.U., Hunter, N., and Kleckner, N. (2002). Physical and functional interactions among basic chromosome organizational features govern early steps of meiotic chiasma formation. Cell 111, 791–802.

Borde, V., and Cobb, J. (2009). Double functions for the Mre11 complex during DNA double-strand break repair and replication. Int. J. Biochem. Cell Biol. 41, 1249–1253.

Borde, V., Robine, N., Lin, W., Bonfils, S., Géli, V., and Nicolas, A. (2009). Histone H3 lysine 4 trimethylation marks meiotic recombination initiation sites. EMBO J. 28, 99–111.

Borner, G. V., Barot, A., and Kleckner, N. (2008). Yeast Pch2 promotes domainal axis organization, timely recombination progression, and arrest of defective recombinosomes during meiosis. Proc. Natl. Acad. Sci. 105, 3327–3332.

Brown, S.D., Jarosinska, O.D., and Lorenz, A. (2018). Genetic interactions between the chromosome axis-associated protein Hop1 and homologous recombination determinants in *Schizosaccharomyces pombe*. Curr. Genet. 64, 1089–1104.

Carballo, J.A., Johnson, A.L., Sedgwick, S.G., and Cha, R.S. (2008). Phosphorylation of the axial element protein Hop1 by Mec1/Tel1 ensures meiotic interhomolog recombination. Cell 132, 758–770.

Carballo, J.A., Panizza, S., Serrentino, M.E., Johnson, A.L., Geymonat, M., Borde, V., Klein, F., and Cha, R.S. (2013). Budding yeast ATM/ATR control meiotic double-strand break (DSB) levels by down-regulating Rec114, an essential component of the DSB-machinery. PLoS Genet. 9. e1003545

Couteau, F., and Zetka, M. (2005). HTP-1 coordinates synaptonemal complex assembly with homolog alignment during meiosis in *C. elegans*. Genes Dev. 19, 2744–2756.

Couteau, F., Nabeshima, K., Villeneuve, A., and Zetka, M. (2004). A component of *C. elegans* meiotic chromosome axes at the interface of homolog alignment, synapsis, nuclear reorganization, and recombination. Curr. Biol. 14, 585–592.

Daniel, K., Lange, J., Hached, K., Fu, J., Anastassiadis, K., Roig, I., Cooke, H.J., Stewart, A.F., Wassmann, K., Jasin, M., et al. (2011). Meiotic homologue alignment and its quality surveillance are controlled by mouse HORMAD1. Nat. Cell Biol. 13, 599–610.

Ding, D.Q., Sakurai, N., Katou, Y., Itoh, T., Shirahige, K., Haraguchi, T., and Hiraoka, Y. (2006). Meiotic cohesins modulate chromosome compaction during meiotic prophase in fission yeast. J. Cell Biol. 174, 499–508.

Ellermeier, C., and Smith, G.R. (2005). Cohesins are required for meiotic DNA breakage and recombination in *Schizosaccharomyces pombe*. Proc. Natl. Acad. Sci. 102, 10952–10957.

Evans, D.H., Li, Y.F., Fox, M.E., and Smith, G.R. (1997). A WD repeat protein, Rec14, essential for meiotic recombination in *Schizosaccharomyces pombe*. Genetics 146, 1253–1264.

Feng, J., Fu, S., Cao, X., Wu, H., Lu, J., Zeng, M., Liu, L., Yang, X., and Shen, Y. (2017). Synaptonemal complex protein 2 (SYCP2) mediates the association of the centromere with the synaptonemal complex. Protein & cell, 8(7), 538-543.

Ferdous, M., Higgins, J.D., Osman, K., Lambing, C., Roitinger, E., Mechtler, K., Armstrong, S.J., Perry, R., Pradillo, M., Cuñado, N., et al. (2012). Inter-homolog crossing-over and synapsis in *arabidopsis* meiosis are dependent on the chromosome axis protein AtASY3. PLoS Genet. 8. e1002507

Fukuda, T., Daniel, K., Wojtasz, L., Toth, A., and Höög, C. (2010). A novel mammalian HORMA domain-containing protein, HORMAD1, preferentially associates with unsynapsed meiotic chromosomes. Exp. Cell Res. 316, 158–171.

Furuse, M., Nagase, Y., Tsubouchi, H., Murakami-Murofushi, K., Shibata, T., and Ohta, K. (1998). Distinct roles of two separable in vitro activities of yeast Mre11 in mitotic and meiotic recombination. EMBO J. 17, 6412–6425.

Garcia, V., Gray, S., Allison, R.M., Cooper, T.J., and Neale, M.J. (2015). Tel1ATM-mediated interference suppresses clustered meiotic double-strand-break formation. Nature 520, 114–118.

Gregan, J., Rabitsch, P.K., Sakem, B., Csutak, O., Latypov, V., Lehmann, E., Kohli, J., and Nasmyth, K. (2005). Novel genes required for meiotic chromosome segregation are identified by a high-throughput knockout screen in fission yeast. Curr. Biol. 15, 1663–1669.

Grelon, M., Vezon, D., Gendrot, G., and Pelletier, G. (2001). AtSPO11-1 is necessary for efficient meiotic recombination in plants. EMBO J. 20, 589–600.

Grey, C., Baudat, F., and de Massy, B. (2018). PRDM9, a driver of the genetic map. PLOS Genet. 14, e1007479.

Henderson, K.A., Kee, K., Maleki, S., Santini, P.A., and Keeney, S. (2006). Cyclin-Dependent Kinase Directly Regulates Initiation of Meiotic Recombination. Cell 125, 1321–1332.

Hollingsworth, N.M., and Byers, B. (1989). HOP1: a yeast meiotic pairing gene. Genetics 121, 445–462.

Hollingsworth, N.M., Goetsch, L., and Byers, B. (1990). The HOP1 gene encodes a meiosis-specific component of yeast chromosomes. Cell 61, 73–84.

Ishiguro, K.I., Kim, J., Fujiyama-Nakamura, S., Kato, S., and Watanabe, Y. (2011). A new meiosis-specific cohesin complex implicated in the cohesin code for homologous pairing. EMBO Rep. 12, 267–275.

Ito, M., Kugou, K., Fawcett, J.A., Mura, S., Ikeda, S., Innan, H., and Ohta, K. (2014). Meiotic recombination cold spots in chromosomal cohesion sites. Genes to Cells 19, 359–373.

Jolivet, S., Vezon, D., Froger, N., and Mercier, R. (2006). Non conservation of the meiotic function of the Ski8/Rec103 homolog in *Arabidopsis*. Genes to Cells 11, 615–622.

Joshi, N., Barot, A., Jamison, C., and Börner, G.V. (2009). Pch2 links chromosome axis remodeling at future crossover sites and crossover distribution during yeast meiosis. PLoS Genet. 5, e1000557.

Kee, K., Protacio, R.U., Arora, C., and Keeney, S. (2004). Spatial organization and dynamics of the association of Rec102 and Rec104 with meiotic chromosomes. EMBO J. 23, 1815–1824.

Keeney, S., Giroux, C.N., and Kleckner, N. (1997). Meiosis-Specific DNA Double-Strand Breaks Are Catalyzed by Spo11, a Member of a Widely Conserved Protein Family. Cell 88, 375–384.

Kim, K.P., Weiner, B.M., Zhang, L., Jordan, A., Dekker, J., and Kleckner, N. (2010). Sister cohesion and structural axis components mediate homolog bias of meiotic recombination. Cell 143, 924–937.

Kim, Y., Rosenberg, S.C., Kugel, C.L., Kostow, N., Rog, O., Davydov, V., Su, T.Y., Dernburg, A.F., and Corbett, K.D. (2014). The chromosome axis controls meiotic events through a hierarchical assembly of HORMA domain proteins. Dev. Cell 31, 487–502.

Kitajima, T.S., Yokobayashi, S., Yamamoto, M., and Watanabe, Y. (2003). Distinct cohesin complexes organize meiotic chromosome domains. Science. 300, 1152–1155.

Kleckner, N. (2006). Chiasma formation: Chromatin/axis interplay and the role(s) of the synaptonemal complex. Chromosoma 115, 175–194.

Klein, F., Mahr, P., Galova, M., Buonomo, S.B.C., Michaelis, C., Nairz, K., and Nasmyth, K. (1999). A central role for cohesins in sister chromatid cohesion, formation of axial elements, and recombination during yeast meiosis. Cell 98, 91–103.

Kugou, K., Fukuda, T., Yamada, S., Ito, M., Sasanuma, H., Mori, S., Katou, Y., Itoh, T., Matsumoto, K., Shibata, T., et al. (2009). Rec8 guides canonical Spo11 distribution along yeast meiotic chromosomes. Mol. Biol. Cell 20, 3064–3076.

Kumar, R., Bourbon, H.M., and De Massy, B. (2010). Functional conservation of Mei4 for meiotic DNA double-strand break formation from yeasts to mice. Genes Dev. 24, 1266–1280.

Lam, I., and Keeney, S. (2015). Mechanism and regulation of meiotic recombination initiation. Cold Spring Harb. Perspect. Biol. 7, a016634.

Latypov, V., Rothenberg, M., Lorenz, A., Octobre, G., Csutak, O., Lehmann, E., Loidl, J., and Kohli, J. (2010). Roles of Hop1 and Mek1 in Meiotic Chromosome Pairing and Recombination Partner Choice in *Schizosaccharomyces pombe*. Mol. Cell. Biol. 30, 1570–1581.

Lee, J., and Hirano, T. (2011). RAD21L, a novel cohesin subunit implicated in linking homologous chromosomes in mammalian meiosis. J. Cell Biol. 192, 263–276.

Libby, B.J., Reinholdt, L.G., and Schimenti, J.C. (2003). Positional cloning and characterization of Mei1, a vertebrate-specific gene required for normal meiotic chromosome synapsis in mice. Proc. Natl. Acad. Sci. 100, 15706–15711.

Lin, Y., Larson, K.L., Dorer, R., and Smith, G.R. (1992). Meiotically induced *rec7* and *rec8* genes of *Schizosaccharomyces pombe*. Genetics 132, 75–85.

Lorenz, A. (2004). *S. pombe* meiotic linear elements contain proteins related to synaptonemal complex components. J. Cell Sci. 117, 3343–3351.

Ludin, K., Mata, J., Watt, S., Lehmann, E., Bähler, J., and Kohli, J. (2008). Sites of strong Rec12/Spo11 binding in the fission yeast genome are associated with meiotic recombination and with centromeres. Chromosoma 117, 431–444.

Mao-Draayer, Y., Galbraith, A.M., Pittman, D.L., Cool, M., and Malone, R.E. (1996). Analysis of meiotic recombination pathways in the yeast *Saccharomyces cerevisiae*. Genetics 144, 71–86.

Medhi, D., Goldman, A.S.H., and Lichten, M. (2016). Local chromosome context is a major determinant of crossover pathway biochemistry during budding yeast meiosis. Elife 5, 1–20.

Miyoshi, T., Ito, M., Kugou, K., Yamada, S., Furuichi, M., Oda, A., Yamada, T., Hirota, K., Masai, H., and Ohta, K. (2012). A central coupler for recombination initiation linking chromosome architecture to S phase checkpoint. Mol. Cell 47, 722–733.

Molnar, M. (2003). Linear element formation and their role in meiotic sister chromatid cohesion and chromosome pairing. J. Cell Sci. 116, 1719–1731.

Molnar, M., Bahler, J., Sipiczki, M., and Kohli, J. (1995). The *rec8* gene of *Schizosaccharomyces pombe* is involved in linear element formation, chromosome pairing and sister-chromatid cohesion during meiosis. Genetics 141, 61–73.

Muller, H., Scolari, V.F., Agier, N., Piazza, A., Thierry, A., Mercy, G., Descorps‐Declere, S., Lazar‐Stefanita, L., Espeli, O., Llorente, B., et al. (2018). Characterizing meiotic chromosomes' structure and pairing using a designer sequence optimized for Hi‐C. Mol. Syst. Biol. 14, e8293.

Murakami, H., and Keeney, S. (2014). Temporospatial coordination of meiotic dna replication and recombination via DDK recruitment to replisomes. Cell 158, 861–873.

De Muyt, A., Vezon, D., Gendrot, G., Gallois, J.L., Stevens, R., and Grelon, M. (2007). AtPRD1 is required for meiotic double strand break formation in *Arabidopsis thaliana*. EMBO J. 26, 4126–4137.

Neale, M.J., Pan, J., and Keeney, S. (2005). Endonucleolytic processing of covalent protein-linked DNA double-strand breaks. Nature 436, 1053–1057.

Niu, H., Wan, L., Baumgartner, B., Schaefer, D., Loidl, J., and Hollingsworth, N.M. (2005). Partner choice during meiosis is regulated by Hop1-promoted dimerization of Mek1. Mol. Biol. Cell 16, 5804–5818.

Offenberg, H.H., Schalk, J.A.C., Meuwissen, R.L.J., Van Aalderen, M., Kester, H.A., Dietrich, A.J.J., and Heyting, C. (1998). SCP2: A major protein component of the axial elements of synaptonemal complexes of the rat. Nucleic Acids Res. 26, 2572–2579.

Ohta, K., Shibata, T., and Nicolas, A. (1994). Changes in chromatin structure at recombination initiation sites during yeast meiosis. Embo J 13, 5754–5763.

Pan, J., Sasaki, M., Kniewel, R., Murakami, H., Blitzblau, H.G., Tischfield, S.E., Zhu, X., Neale, M.J., Jasin, M., Socci, N.D., et al. (2011). A hierarchical combination of factors shapes the genome-wide topography of yeast meiotic recombination initiation. Cell 144, 719–731.

Panizza, S., Mendoza, M.A., Berlinger, M., Huang, L., Nicolas, A., Shirahige, K., and Klein, F. (2011). Spo11-accessory proteins link double-strand break sites to the chromosome axis in early meiotic recombination. Cell 146, 372–383.

Parisi, S., McKay, M.J., Molnar, M., Thompson, M.A., van der Spek, P.J., van Drunen-Schoenmaker, E., Kanaar, R., Lehmann, E., Hoeijmakers, J.H.J., and Kohli, J. (1999). Rec8p, a meiotic recombination and sister chromatid cohesion phosphoprotein of the Rad21p family conserved from fission yeast to humans. Mol. Cell. Biol. 19, 3515–3528.

Robert, T., Nore, A., Brun, C., Maffre, C., Crimi, B., Guichard, V., Bourbon, H.M., and De Massy, B. (2016). The Topo VIB-Like protein family is required for meiotic DNA double-strand break formation. Science.351, 943–949.

Rockmill, B., and Roeder, G.S. (1988). RED1: a yeast gene required for the segregation of chromosomes during the reductional division of meiosis. Proc. Natl. Acad. Sci. U. S. A. 85, 6057–6061.

Rockmill, B., and Roeder, G.S. (1991). A meiosis-specific protein kinase homolog required for chromosome synapsis and recombination. Genes Dev. 5, 2392–2404.

Rosenberg, S.C., and Corbett, K.D. (2015). The multifaceted roles of the HORMA domain in cellular signalling. J. Cell Biol. 211, 745–755.

Rothenberg, M., Kohli, J., and Ludin, K. (2009). Ctp1 and the MRN-complex are required for endonucleolytic Rec12 removal with release of a single class of oligonucleotides in fission yeast. PLoS Genet. 5, e1000722.

Sanchez-Moran, E., Santos, J.L., Jones, G.H., and Franklin, F.C.H. (2007). ASY1 mediates AtDMC1-dependent interhomolog recombination during meiosis in *Arabidopsis*. Genes Dev. 21, 2220–2233.

Sasanuma, H., Hirota, K., Fukuda, T., Kakusho, N., Kugou, K., Kawasaki, Y., Shibata, T., Masai, H., and Ohta, K. (2008). Cdc7-dependent phosphorylation of Mer2 facilitates initiation of yeast meiotic recombination. Genes Dev. 22, 398–410.

Stanzione, M., Baumann, M., Papanikos, F., Dereli, I., Lange, J., Ramlal, A., Tränkner, D., Shibuya, H., De Massy, B., Watanabe, Y., et al. (2016). Meiotic DNA break formation requires the unsynapsed chromosome axis-binding protein IHO1 (CCDC36) in mice. Nat. Cell Biol. 18, 1208–1220.

Sym, M., Engebrecht, J.A., and Roeder, G.S. (1993). ZIP1 is a synaptonemal complex protein required for meiotic chromosome synapsis. Cell 72, 365–378.

Tessé, S., Bourbon, H.M., Debuchy, R., Budin, K., Dubois, E., Liangran, Z., Antoine, R., Piolot, T., Kleckner, N., Zickler, D., et al. (2017). Asy2/Mer2: An evolutionarily conserved mediator of meiotic recombination, pairing, and global chromosome compaction. Genes Dev. 31, 1880–1893.

Usui, T., Ohta, T., Oshiumi, H., Tomizawa, J.I., Ogawa, H., and Ogawa, T. (1998). Complex formation and functional versatility of Mre11 of budding yeast in recombination. Cell 95, 705–716.

Vrielynck, N., Chambon, A., Vezon, D., Pereira, L., Chelysheva, L., De Muyt, A., Mézard, C., Mayer, C., and Grelon, M. (2016). A DNA topoisomerase VI-like complex initiates meiotic recombination. Science.351, 939–943.

Watanabe, Y., and Nurse, P. (1999). Cohesin Rec8 is required for reductional chromosome segregation at meiosis. Nature 400, 461–464.

West,A.M.V., Komives,E.A. and Corbett,K.D. (2018) Conformational dynamics of the Hop1 HORMA domain reveal a common mechanism with the spindle checkpoint protein Mad2. Nucleic Acids Res., 46, 279–292.

West, A.M. V, Rosenberg, S.C., Ur, S.N., Lehmer, M.K., Ye, Q., Hagemann, G., Caballero, I., Usón, I., MacQueen, A.J., Herzog, F., et al. (2019). A conserved filamentous assembly underlies the structure of the meiotic chromosome axis. Elife *8*, e40372.

Wojtasz, L., Daniel, K., Roig, I., Bolcun-Filas, E., Xu, H., Boonsanay, V., Eckmann, C.R., Cooke, H.J., Jasin, M., Keeney, S., et al. (2009). Mouse HORMAD1 and HORMAD2, two conserved meiotic chromosomal proteins, are depleted from synapsed chromosome axes with the help of TRIP13 AAA-ATPase. PLoS Genet. 5, e1000702.

Woltering,D., Baumgartner,B., Bagchi,S., Larkin,B., Loidl,J., Santos,T.D.L. and Hollingsworth,N.M. (2000) Recombination Checkpoint Functions Require Physical Interaction between the Chromosomal Proteins Red1p and Hop1p. Mol. Cell. Biol., 20, 6646–6658.

Wu, T.C., and Lichten, M. (1994). Meiosis-induced double-strand break sites determined by yeast chromatin structure. Science.263, 515–518.

Xu, H., Beasley, M.D., Warren, W.D., van der Horst, G.T.J., and McKay, M.J. (2005). Absence of mouse REC8 cohesin promotes synapsis of sister chromatids in meiosis. Dev. Cell 8, 949–961.

Xu, L., Weiner, B.M., and Kleckner, N. (1997). Meiotic cells monitor the status of the interhomolog recombination complex. Genes Dev. 11, 106–118.

Yamada, S., Ohta, K., and Yamada, T. (2013). Acetylated Histone H3K9 is associated with meiotic recombination hotspots, and plays a role in recombination redundantly with other factors including the H3K4 methylase Set1 in fission yeast. Nucleic Acids Res. 41, 3504–3517.

Yamada, T., Mizuno, K.I., Hirota, K., Kon, N., Wahls, W.P., Hartsuiker, E., Murofushi, H., Shibata, T., and Ohta, K. (2004). Roles of histone acetylation and chromatin remodelling factor in a meiotic recombination hotspot. EMBO J. 23, 1792–1803.

Zickler, D., and Kleckner, N. (2015). Recombination, pairing, and synapsis of homologs during meiosis. Cold Spring Harb. Perspect. Biol. 7, 1–28

7. Acknowledgement

I would like to express my deepest appreciation to Professor Kunihiro Ohta, who gave me a lot of advice, training, the opportunity to go international conference, and every support for accomplishing my research. I also would like to thank Dr. Arisa Oda, who guided my computational research from scratch. I greatly appreciate Dr. Takatomi Yamada, who intensively revised the manuscript of the paper.

I am grateful to Dr. Masaru Ito for the discussion and instruction of co-immunoprecipitation and data analysis of ChIP sequence; Dr. Takahiro Nakamura for the instruction of pulsed field gel electrophoresis; Ms. Emi Takaya for supporting experiments. I would also like to thank all the members of Ohta lab who supported me with a friendly atmosphere.

I also applicate to Dr. Yoshinori Watanabe and Dr. Takeshi Sakuno for antibody, plasmids, and educational training of my experiments and science for five years. I also thank Dr. Tomoichiro Miyoshi for fission yeast strain and plasmids.

Finally, I would like to express my sincere appreciation to my family for every supporting my seven years of graduate research.

The research in this thesis has been accepted for publication in Nucleic Acids Research Published by Oxford University Press.